First measurement of Λ_c^+ production down to $p_T = 0$ in pp and p-Pb collisions at $\sqrt{s_{NN}} = 5.02$ TeV

S. Acharya *et al.*[*]
(ALICE Collaboration)

The production of prompt Λ_c^+ baryons has been measured at midrapidity in the transverse momentum interval $0 < p_T < 1$ GeV/c for the first time, in pp and p–Pb collisions at a center-of-mass energy per nucleon-nucleon collision $\sqrt{s_{NN}} = 5.02$ TeV. The measurement was performed in the decay channel $\Lambda_c^+ \to pK_S^0$ by applying new decay reconstruction techniques using a Kalman-Filter vertexing algorithm and adopting a machine-learning approach for the candidate selection. The p_T-integrated Λ_c^+ production cross sections in both collision systems were determined and used along with the measured yields in Pb–Pb collisions to compute the p_T-integrated nuclear modification factors $R_{p\text{Pb}}$ and R_{AA} of Λ_c^+ baryons, which are compared to model calculations that consider nuclear modification of the parton distribution functions. The Λ_c^+/D^0 baryon-to-meson yield ratio is reported for pp and p–Pb collisions. Comparisons with models that include modified hadronization processes are presented, and the implications of the results on the understanding of charm hadronization in hadronic collisions are discussed. A significant (3.7σ) modification of the mean transverse momentum of Λ_c^+ baryons is seen in p–Pb collisions with respect to pp collisions, while the p_T-integrated Λ_c^+/D^0 yield ratio was found to be consistent between the two collision systems within the uncertainties.

I. INTRODUCTION

Measurements of heavy-flavor hadron production in hadronic collisions provide crucial tests for calculations based on quantum chromodynamics (QCD). Typically, calculations of p_T-differential heavy-flavor hadron production cross sections in hadronic collisions are factorized into three separate components: the parton distributions functions (PDFs), which describe the Bjorken-x distributions of quarks and gluons within the incoming hadrons; the hard-scattering cross section for the partons to produce a charm or beauty quark; and the fragmentation functions, which characterize the hadronization of a quark to a given hadron species [1]. As charm and beauty quarks have masses much larger than the Λ_{QCD} energy scale, the parton-parton hard-scattering cross sections can be calculated perturbatively [2]. In contrast, the fragmentation functions cannot be calculated with perturbative QCD (pQCD) methods, and so must be determined from measurements in e^+e^- collisions. They are then applied in cross section calculations under the assumption that the relevant hadronization processes are "universal", i.e., independent of the collision system. Hadron-to-hadron production ratios within the charm sector, such as D_s^+/D^0 and Λ_c^+/D^0, are therefore especially effective for probing hadronization

*Full author list given at the end of the article.

effects, since in theoretical calculations the PDFs and partonic interaction cross sections are common to all charm-hadron species and their effects almost fully cancel in the yield ratios.

Previous measurements of charm-meson production cross sections in pp collisions at the CERN Large Hadron Collider (LHC) [3–6] show that the D^+/D^0 and D_s^+/D^0 ratios are independent of the transverse momentum (p_T) within uncertainties, and are consistent with results from e^+e^- and e^-p collisions [7]. The ratios are also described well by the PYTHIA 8 event generator using the Monash tune [8,9], which adopts hadronization fractions based on fragmentation functions from e^+e^- collisions. However, the charm baryon-to-meson ratios Λ_c^+/D^0, $\Xi_c^{0,+}/D^0$, Ω_c^0/D^0, and $\Sigma_c^{0,++}/D^0$ measured at midrapidity at the LHC [10–17] show significant deviations from the values measured in e^+e^- collisions, and the Monash tune of PYTHIA significantly underpredicts the production rates of charm baryons. Further hadronization effects apart from pure in-vacuum fragmentation must therefore be considered in order for models to better describe the Λ_c^+ measurements. These effects include color reconnection beyond the leading-color approximation in PYTHIA 8 [18], quark coalescence effects such as those applied in the Catania model [19] and in the quark (re)combination model (QCM) [20], or variations of the statistical hadronization model (SHM) including feed-down to the ground-state baryon species from the decays of yet-unmeasured resonant states predicted by the relativistic quark model (RQM) [21]. However, for the heavier charm-strange baryon states $\Xi_c^{0,+}$ and Ω_c^0 [15,17], only the Catania model is able to adequately describe the data. Measurements of beauty-baryon production in pp collisions by the CMS and LHCb Collaborations [22–24] also indicate similar differences in hadronization mechanisms in

the beauty sector between hadronic and leptonic collision systems.

Differences between leptonic and hadronic collision systems are further highlighted by the measured fragmentation fractions of ground-state single-charm hadrons, as reported at midrapidity for pp collisions at center-of-mass energy $\sqrt{s} = 5.02$ TeV in Ref. [25], where a significant enhancement of Λ_c^+ and $\Xi_c^{0,+}$ is seen with respect to e^+e^- and e^-p collisions, along with a corresponding depletion of the relative fraction of D mesons. However, the determination of these fragmentation fractions is dependent on model assumptions, as the evaluation of the p_T-integrated production cross sections of Λ_c^+ and $\Xi_c^{0,+}$ baryons required an extrapolation in order to cover regions of phase space that were not possible to study experimentally. This is especially relevant in the low-p_T region, where a significant fraction of the overall production of charm hadrons occurs and the uncertainties on the factorization and renormalization scales of pQCD calculations used for the extrapolation become large. Measuring down to low p_T is highly challenging, due to the smaller displacement of the decay vertex from the interaction vertex, limiting the effectiveness of topological selections due to the finite detector resolution. This necessitates the use of alternative reconstruction and selection techniques to extract a significant signal from the combinatorial background.

Charm hadrons are also studied in p–Pb collisions at the LHC in order to examine possible modifications of their production due to the presence of a cold nuclear environment. The nuclear modification factor, $R_{p\mathrm{Pb}}$, of D mesons measured by ALICE in p–Pb collisions at center-of-mass energy per nucleon-nucleon collision $\sqrt{s_{NN}} = 5.02$ TeV is consistent with unity for $0 < p_T < 36$ GeV/c [26], suggesting that the cold nuclear matter effects that influence charm-hadron production at midrapidity are moderate. However, measurements of Λ_c^+ baryons in p–Pb collisions [11] indicate a p_T-dependent modification with respect to D mesons, with an $R_{p\mathrm{Pb}}$ lower than unity for $1 < p_T < 2$ GeV/c and systematically above unity for $p_T > 2$ GeV/c. This result is consistent with an increase in the mean p_T of charm baryons in p–Pb collisions with respect to pp collisions. Similar effects have been observed in differential studies of Λ_c^+ and D^0 production as a function of charged-particle multiplicity in pp collisions at $\sqrt{s} = 13$ TeV by ALICE [27], where the p_T dependence of the Λ_c^+/D^0 ratio was significantly modified in high-multiplicity collisions with respect to low-multiplicity collisions without any significant effect on the p_T-integrated Λ_c^+/D^0 ratio. This can be extended by studying highly peripheral Pb–Pb collisions, where the multiplicity densities of charged particles coincide with the highest multiplicity classes in pp collisions at $\sqrt{s} = 13$ TeV. The Λ_c^+/D^0 ratios measured by the LHCb Collaboration in peripheral Pb–Pb collisions at forward rapidity [28] exhibit a significant p_T dependence, albeit with systematically lower values than those measured in the same p_T region at midrapidity. However, when these are calculated after integrating in the visible p_T region, they do not have any significant dependence on the number of nucleons participating in the collision, $\langle N_{\mathrm{part}} \rangle$, reaffirming the independence of the baryon-to-meson ratio on the multiplicity. A modification of the p_T shape as a function of multiplicity has also

been observed in the strangeness sector by the ALICE and CMS Collaborations [29,30] and is consistent with the effect of radial flow in hydrodynamic models such as EPOS LHC [31]. In this picture, particles of larger mass are boosted to higher transverse momenta due to the presence of a common velocity field [32]. Furthermore, baryon production may be enhanced as a result of hadronization by quark recombination [33]. This can be further examined by extending the measurement of Λ_c^+-baryon production down to $p_T = 0$ in both collision systems and determining the mean transverse momentum. In addition, comparisons between p–Pb and Pb–Pb collisions make it possible to disentangle initial- and final-state nuclear effects on charm-baryon production in heavy-ion collisions. The effect of nuclear shadowing [34], which arises due to a modification of the nuclear PDFs, can lead to a reduction in the charm-hadron yields at low p_T due to a reduction of parton densities at low Bjorken-x. The nuclear modification factor R_{AA} of Λ_c^+ baryons at midrapidity in central Pb–Pb collisions at $\sqrt{s_{NN}} = 5.02$ TeV has a value systematically lower than unity for $p_T < 4$ GeV/c, where nuclear shadowing is expected to play a relevant role, and $p_T > 6$ GeV/c [35], as expected from parton energy loss in the quark-gluon plasma created in the collision, while for $4 < p_T < 6$ GeV/c it is consistent with unity. Measurements by the CMS Collaboration in the region $10 < p_T < 20$ GeV/c [13] confirm this suppression at high p_T, with an indication of increased suppression for central (0–30%) compared to peripheral (30–100%) collisions. Studying the p_T-integrated nuclear modification factors allows us to determine whether the modification of the production yields observed in specific p_T regions is due to a reduction of the overall Λ_c^+ yield, or a modification of the momentum spectra in different collision systems.

In this article, new measurements of Λ_c^+-baryon production in the p_T region $0 < p_T < 1$ GeV/c in pp and p–Pb collisions at $\sqrt{s_{NN}} = 5.02$ TeV are reported. With respect to the previously published Λ_c^+ production cross sections [11,12], the measurements in both systems are extended down to $p_T = 0$ thanks to new decay reconstruction techniques, which employ a Kalman-Filter (KF) vertexing algorithm [36] coupled with machine-learning-based selections [37]. The p_T-integrated Λ_c^+ production cross sections and Λ_c^+/D^0 ratios reported in Ref. [11] are updated using these results, and the p_T-integrated nuclear modification factor $R_{p\mathrm{Pb}}$ is calculated. The new values are obtained without requiring a model-dependent extrapolation in the $0 < p_T < 1$ GeV/c interval. The measurement of the full momentum spectrum also enables the calculation of the mean p_T of Λ_c^+ baryons in pp and p–Pb collisions. The integrated production cross section in pp collisions is used along with the measured Λ_c^+ yields in Pb–Pb collisions [35] in order to derive the p_T-integrated nuclear modification factor R_{AA}. The paper is organized as follows. Section II describes the ALICE apparatus and the analysed data samples. Section III details the analysis methods that were used. Sections IV and V outline the corrections that are applied to calculate the Λ_c^+ production cross sections, and the sources of systematic uncertainty. The results are presented in Sec. VI and compared with model calculations. Finally, a brief summary is given in Sec. VII.

II. EXPERIMENTAL SETUP AND DATA SAMPLES

The ALICE detector system and its performance are described in detail in Refs. [38,39]. The reconstruction of charm baryons from their hadronic decay products at midrapidity primarily relies on the Inner Tracking System (ITS) [40], the Time Projection Chamber (TPC) [41], and the time-of-flight detector (TOF) [42] for tracking, primary and decay vertex reconstruction, and charged-particle identification (PID). These detectors are located inside a solenoidal magnet of field strength 0.5 T. In addition, the V0 scintillator arrays [43] are used for triggering collision events and for determining the luminosity when used in conjunction with the T0 detector [44], and the Zero-Degree Calorimeter (ZDC) is employed for offline event rejection in p–Pb collisions [39].

The analysis was performed at midrapidity on data from pp and p–Pb collisions at $\sqrt{s_{NN}} = 5.02$ TeV collected with a minimum-bias (MB) trigger during Run 2 of the LHC. For pp collisions, the results are quoted for $|y| < 0.5$, whereas for p–Pb collisions the rapidity in the nucleon–nucleon center-of-mass system ($y_{\rm cms}$) is shifted due to the asymmetry of the colliding beams, corresponding to a rapidity range of $-0.04 < y_{\rm cms} < 0.96$.

The MB trigger requires a pair of coincident signals in the two V0 scintillator arrays. Further offline selections were applied to suppress the background originating from beam-gas collisions and other machine-related background sources [45]. In order to maintain uniform ITS acceptance in pseudorapidity, only events with a reconstructed vertex position within 10 cm along the beam axis from the nominal interaction point were analyzed. The primary vertex position was identified using tracks reconstructed in the TPC and ITS detectors. Events with multiple interaction vertices due to pileup from several collisions were removed using an algorithm based on tracks reconstructed with the TPC and ITS detectors [39]. Using these selection criteria, the sample of pp collisions comprised approximately one billion events, corresponding to an integrated luminosity of $\mathcal{L}_{\rm int} = 19.5 \pm 0.4$ nb^{-1} [46], while in p–Pb collisions approximately 6×10^8 events were selected, corresponding to $\mathcal{L}_{\rm int} = 287 \pm 11$ μb^{-1} [47].

III. ANALYSIS METHODS

In this analysis, Λ_c^+ baryons were reconstructed via the decay channel $\Lambda_c^+ \to pK_S^0$ and respective charge conjugates, with branching ratio BR $= (1.59 \pm 0.08)\%$, followed by the subsequent decay $K_S^0 \to \pi^+\pi^-$, BR $= (69.2 \pm 0.05)\%$ [48]. The contributions from both Λ_c^+ and $\overline{\Lambda}_c^-$ were taken into account in the measurements; for brevity, both are referred to collectively as "Λ_c^+" in this article. Charged-particle tracks and particle-decay vertices were reconstructed in the central barrel using the ITS and the TPC. The particle trajectories in the vicinity of the primary vertex, and the decay vertices, were reconstructed with the KFParticle package [36], which allows a direct estimate of their parameters and the associated uncertainties. The K_S^0 candidate was reconstructed by pairing opposite-sign charged tracks forming a neutral decay vertex displaced from the primary vertex. This candidate was then paired with a proton-candidate track, originating from the primary vertex, to form a Λ_c^+ candidate.

To ensure good quality of the tracks used to reconstruct the Λ_c^+ candidates, further selection criteria were applied in addition to the event selections mentioned above. In order to maintain a uniform detector acceptance, the tracks of the charged particles involved in the decay chain were required to be within the pseudorapidity interval $|\eta| < 0.8$. The number of clusters in the TPC used for the energy loss determination was required to be larger than 50, to enhance the precision of the mean specific energy loss (dE/dx). Furthermore, for the track reconstruction, the minimum required number of crossed rows in the TPC was 70 out of a possible 159. Primary proton candidates were required to have a minimum of four (out of a maximum of six) hits in the ITS.

Several selection criteria on the PID and decay topology were applied to initially filter Λ_c^+ signal candidates. The PID selections were based on the difference between the measured and expected detector signals for a given particle species hypothesis, in units of the detector resolution ($n_\sigma^{\rm det}$). For the pion-candidate tracks from the K_S^0 decay and the proton-candidate track, a selection on the measured dE/dx in the TPC of $|n_\sigma^{\rm TPC}| < 3$ from the respective particle hypothesis was applied. If a measurement in the TOF detector was available, a further TOF PID selection of $|n_\sigma^{\rm TOF}| < 3$ (5) was applied on the particle flight time in p–Pb (pp) collisions. The transverse momentum of the proton was required to be larger than 150 MeV/c. The deviation of the measured invariant mass from the world-average value [48] was required to be within 20 MeV/c^2 for the K_S^0. The Λ_c^+ candidates were also required to have a $\chi^2_{\rm topo}$/NDF < 50, where NDF is the number of degrees of freedom of the topological fit. The $\chi^2_{\rm topo}$/NDF characterises whether the momentum vector of the Λ_c^+ candidate points back to the reconstructed primary vertex, and is calculated by the KFParticle algorithm [36]. A requirement on the distance between the primary and secondary vertices (l) normalized by its uncertainty (Δl) of $l/\Delta l < 30$ was imposed on the Λ_c^+ candidate to filter out decay vertices from longer-living particles. Finally, the estimated proper time ct of the K_S^0 decay and its decay length in the transverse plane were required to be smaller than 50 cm.

After applying the selections described above, the separation between signal and background was optimized using a boosted decision tree (BDT) algorithm. The BDT implementation provided by the XGBoost library was used [37,49]. With the machine learning approach, multiple selection criteria are combined into a single response variable representing the probability of a candidate being a true Λ_c^+ baryon. After the application of a trained BDT model to the full data sample, a selection in the BDT response was applied to reduce the large combinatorial background.

Separate BDT models were trained for each collision system with a sample of signal and background candidates in the interval $0 < p_T < 1$ GeV/c. The signal candidates were obtained from simulated events using the PYTHIA 8.243 [8] Monte Carlo (MC) generator with the Monash tune [9]. The transport of simulated particles within the detector was performed with the GEANT3 package [50], and included a detailed
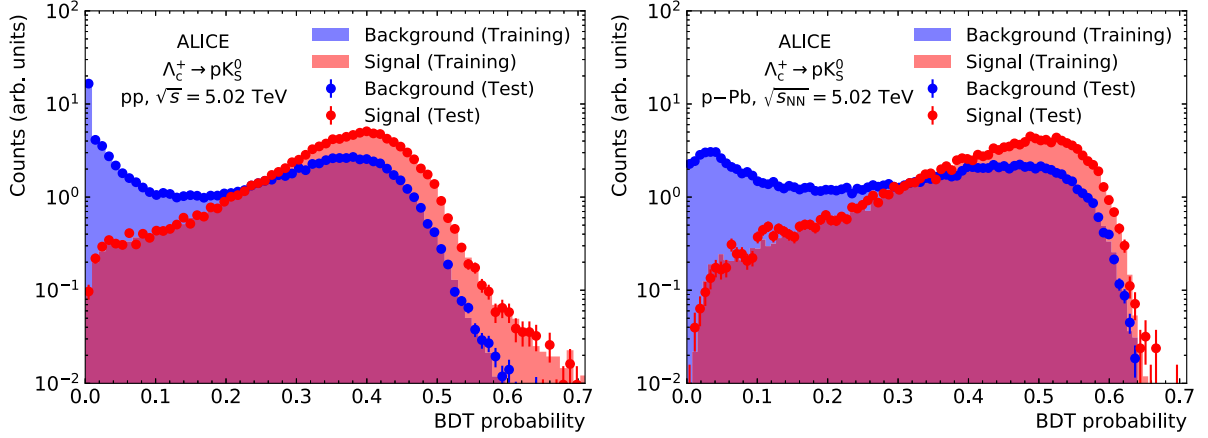
FIG. 1. Distributions of the BDT output probabilities for $\Lambda_c^+ \to pK_S^0$ signal (red) and background (blue) candidates for $0 < p_T < 1$ GeV/c. The left plot shows the model output for pp collisions, and the right plot for p–Pb collisions. The shaded regions represent the output of the training sample, and the markers are the results after applying the model on the test sample.

description of the LHC beam conditions and detector geometry and alignment, as well as the time evolution of the detector configurations during the data taking. For p–Pb collisions, an underlying p–Pb event generated with the HIJING 1.36 generator [51] was added on top of the PYTHIA 8 event to simulate events with more than one nucleon-nucleon collision. Each PYTHIA 8 event was required to contain a charm–anticharm quark pair with at least one of them hadronizing into a Λ_c^+ baryon. Its decay channel was then selected to be the hadronic decay into a proton and a K_S^0. Only prompt Λ_c^+ signal candidates, namely those produced directly in the hadronization of a charm quark or in the strong decay of a directly produced excited charm-hadron state, were selected for the training. Those that were produced in the decay of a particle containing a beauty quark (feed-down) were not used since they have a different decay vertex topology. The background sample was selected from a fraction of real data using the same filtering selections described above, with the additional requirement that the invariant mass of the Λ_c^+ candidate was within the intervals $1.98 < M < 2.23$ GeV/c^2 or $2.34 < M < 2.58$ GeV/c^2 to ensure that the signal region was excluded.

The training variables related to the proton decay track were the n_σ^{TPC} and the track impact parameter with respect to the primary vertex. The training variables describing the topology of the K_S^0 were i) the ct, ii) the decay length in the transverse plane, and iii) the $l/\Delta l$, as defined above. The training variables related to the Λ_c^+ itself were i) the χ_{topo}^2/NDF, ii) the $l/\Delta l$, and iii) the pointing angle, which is defined as the angle between the momentum vector of a particle and the line connecting its production and decay vertices. Figure 1 shows the BDT output probability distribution from the trained model for pp and p–Pb collisions in $0 < p_T < 1$ GeV/c, testing the hypothesis that the candidate belongs to the signal class. The normalized distributions are shown separately for the signal (red) and background (blue) classes, for the training sample (displayed as shaded bars) and the test sample (circles), which is a subset of the input data that was not used for training. The training and test distributions do not deviate significantly, demonstrating that the model is not overtrained. This was further verified using the area under the

receiver operating characteristic curves [52] from the trained models, where for both collision systems a compatible value was found between the training and testing samples. In addition, while the models for the two collision systems peak at different probability values, the overall shape of the BDT output behaves similarly for pp and p–Pb collisions. The proton PID variable and the Λ_c^+ χ_{topo}^2/NDF were found to have the highest importance ranking in the model, estimated using the SHAP package [53], in both collision systems. In addition, the ct of the K_S^0 contributed significantly to the signal and background separation. Despite the limited separation of the two classes, the selection on the BDT output strongly reduces the background contribution while maintaining a high signal efficiency. The BDT probability threshold for a candidate to be selected was optimized to maximise the expected statistical significance. This was calculated using i) an estimated value for the signal in the $0 < p_T < 1$ GeV/c region based on a Lévy-Tsallis fit to the p_T-differential Λ_c^+ production cross sections at higher p_T [11,12], multiplied by the reconstruction and selection efficiencies for each BDT selection threshold, and ii) an estimate of the background within the signal region obtained by interpolating a fit to the invariant mass sidebands using a fraction of the data. The resulting BDT output thresholds were 0.20 for pp collisions, and 0.37 for p–Pb collisions.

After applying the BDT selections, the raw Λ_c^+ yields in the p_T interval $0 < p_T < 1$ GeV/c were obtained by fitting the invariant-mass distributions of the candidates as shown in Fig. 2. The left (right) panel shows the invariant-mass distribution for pp (p–Pb) collisions along with the fit functions. The signal peak was modelled with a Gaussian function and the background was described with a third-order polynomial. The width of the Gaussian distribution was fixed to the value obtained from MC simulations in order to improve the stability of the fit, while the mean was left as a free parameter. To better visualize the line shape of the signal, the invariant mass distributions after subtracting the background fit functions are shown in the lower panels of Fig. 2. The statistical significance of the extracted signal has a value of 3.8 (3.5) for pp (p–Pb) collisions.
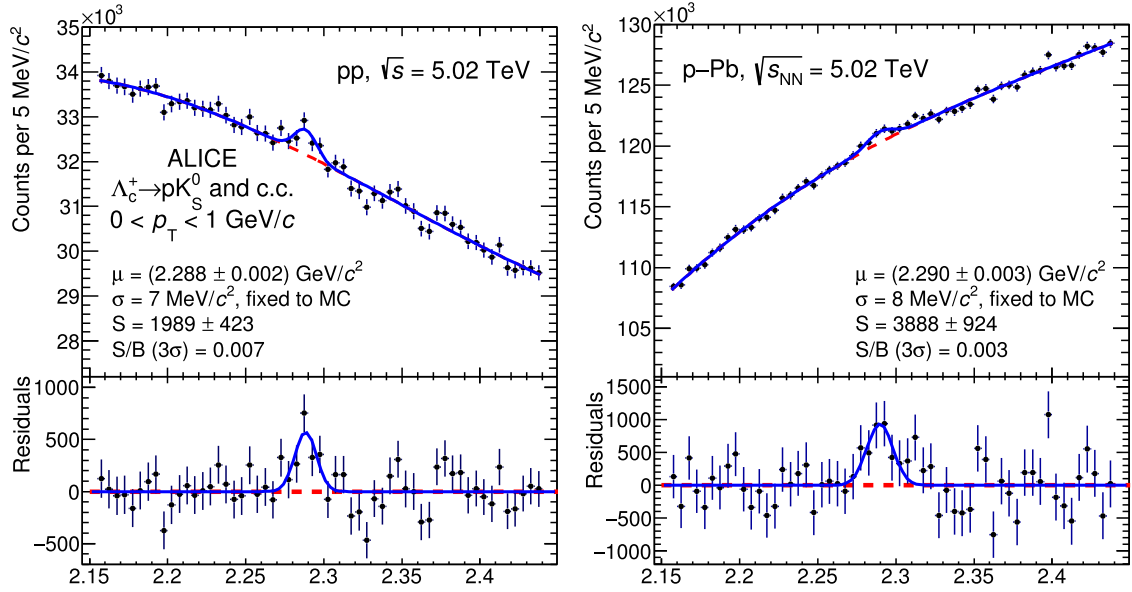
FIG. 2. Invariant mass distributions of $\Lambda_c^+ \to pK_S^0$ candidates in $0 < p_T < 1$ GeV/c, in pp (left) and p–Pb (right) collisions at $\sqrt{s_{NN}} = 5.02$ TeV. The red dashed curves represent the background fits, and the blue curves the total fits. The lower panels show the distributions after subtracting the background estimated with the fit.

IV. CORRECTIONS

The p_T-differential production cross section of prompt Λ_c^+ baryons per unit rapidity in the interval $|y| < 0.5$ for pp collisions and $-0.96 < y_{cms} < 0.04$ for p–Pb collisions was calculated from the raw yields as

$$\frac{d^2\sigma}{dp_T dy} = \frac{1}{2} \frac{f_{prompt}(p_T) \times N_{raw}^{\Lambda_c^+ + \Lambda_c^-}(p_T)}{\Delta y_{lab} \Delta p_T \times (Acc \times \varepsilon)_{prompt}(p_T) \times BR \times \mathscr{L}_{int}},$$
(1)

where $N_{raw}^{\Lambda_c^+ + \Lambda_c^-}$ is the raw yield, f_{prompt} is the fraction of prompt Λ_c^+ in the measured raw yield, BR is the branching ratio, and $\mathscr{L}_{int}$ is the integrated luminosity. The factor 2 accounts for the presence of both particles and antiparticles in the raw yields, and $\Delta y_{lab} \Delta p_T$ accounts for the widths of the rapidity and transverse momentum intervals. For the interval $0 < p_T < 1$ GeV/c, the measurement of Λ_c^+ is performed for $\Delta y_{lab} = 1.6$, under the assumption that the cross section per unit rapidity of Λ_c^+ baryons does not significantly change between $|y_{lab}| < 0.5$ and $|y_{lab}| < 0.8$. This has been verified using PYTHIA 8 [8] and FONLL [2,54] simulations. The factor $(Acc \times \varepsilon)_{prompt}$ is the product of the geometrical acceptance (Acc) and the reconstruction and selection efficiency (ε) for prompt Λ_c^+ candidates in the $\Lambda_c^+ \to pK_S^0$ channel. The $(Acc \times \varepsilon)_{prompt}$ corrections were obtained from MC simulations with the same configuration as those used for the BDT training described above. For both collision systems, the efficiency correction factor was observed to be constant within the interval $0 < p_T < 1$ GeV/c when computed in narrower p_T intervals. The $(Acc \times \varepsilon)_{prompt}$ factor is almost constant as a function of rapidity for $|y_{lab}| < 0.5$, and falls steeply to zero for $|y_{lab}| > 0.5$.

The fraction of the raw Λ_c^+ yield originating from beauty-hadron decays in the selected candidate sample was obtained

following the strategy defined in Ref. [11] using: i) the beauty-meson production cross section from FONLL calculations, which is used as a basis for the p_T shape for all beauty-hadron species [54,55]; ii) the relative abundances of different beauty-hadron species from LHCb measurements in pp collisions [23]; iii) their decay kinematics from PYTHIA 8; and iv) the selection and reconstruction efficiency of Λ_c^+ from beauty-hadron decays, which was estimated from MC simulations. The MC samples were generated with a similar configuration as the training samples described in Sec. III, but instead of a charm-anticharm pair, they included a beauty-antibeauty quark pair in each simulated event, with at least one Λ_c^+ among the decay products of the resulting beauty hadrons. The efficiency is similar between prompt and feed-down candidates, as there are no tight selections applied on the decay topology of the Λ_c^+ baryon. The possible modification of beauty-hadron production in p–Pb collisions was included in the feed-down calculation by scaling the beauty-quark production by a nuclear modification factor $R_{pPb}^{feed-down}$. As for previous ALICE measurements of charm hadrons [11,56], the central value was chosen such that the R_{pPb} of prompt and feed-down Λ_c^+ are equal. The values of $(Acc \times \varepsilon)_{prompt}$, $(Acc \times \varepsilon)_{feed-down}$, and f_{prompt} for $0 < p_T < 1$ GeV/c are listed in Table I for both collision systems.

TABLE I. Correction factors $(Acc \times \varepsilon)_{prompt}$, $(Acc \times \varepsilon)_{feed-down}$, and f_{prompt} in the interval $0 < p_T < 1$ GeV/c within the measured rapidity regions.

	pp	p–Pb
$(Acc \times \varepsilon)_{prompt}$	$(6.30 \pm 0.03)\%$	$(4.77 \pm 0.02)\%$
$(Acc \times \varepsilon)_{feed-down}$	$(6.15 \pm 0.03)\%$	$(4.71 \pm 0.02)\%$
f_{prompt}	$\left(98.2^{+0.9}_{-1.5}\right)\%$	$\left(98.1^{+0.9}_{-3.7}\right)\%$

TABLE II. Systematic uncertainties on the Λ_c^+ production cross section for pp and p–Pb collisions in the p_T interval $0 < p_T < 1$ GeV/c.

	pp	p–Pb
Raw yield extraction	8%	9%
Selection efficiency	9%	9%
Tracking efficiency	4%	6%
Monte Carlo p_T shape	negl.	1%
Feed-down subtraction	$^{+0.9}_{-1.5}$%	$^{+0.9}_{-3.8}$%
Luminosity	2.1%	3.7%
Branching ratio	5%	

V. SYSTEMATIC UNCERTAINTIES

The contributions to the systematic uncertainty on the Λ_c^+ production cross section in $0 < p_T < 1$ GeV/c are summarized in Table II.

The systematic uncertainty on the raw yield extraction was evaluated by repeating the fit to the invariant mass distributions while varying: i) the function used to describe the background, ii) the minimum and maximum of the mass ranges (sidebands) considered for the background fit, iii) the width of the mass peak by $\pm 10\%$ compared to the value obtained from MC, and iv) the width of the mass intervals in the invariant mass distribution. In order to test the sensitivity to the line-shape of the signal, a bin-counting method was used, in which the signal yield was obtained by integrating the invariant-mass distribution after subtracting the background estimated from the fit. The systematic uncertainty was taken as the rms of the resulting raw-yield distribution, which corresponds to 8% (9%) for the analysis in pp (p–Pb) collisions.

The systematic uncertainty on the selection efficiency arises due to possible differences between the real detector resolutions and alignment, and their description in the simulation. This uncertainty was assessed by comparing the production cross sections obtained using different selection criteria. In particular, the selections on the BDT outputs were varied in a range corresponding to a modification of about 30% in the efficiency for both pp and p–Pb collisions. The systematic uncertainty was assigned by adding in quadrature the rms and shift in the mean of the resulting production cross section distribution with respect to the value obtained with the default selections. For both pp and p–Pb collisions, this resulted in an uncertainty of 9%.

The tracking efficiency uncertainty was determined by varying the track quality selection criteria and comparing the matching efficiency between the TPC and ITS in data and MC, as described in Ref. [11]. The uncertainties on the individual tracks were propagated to the Λ_c^+ candidates according to the decay kinematics, resulting in an uncertainty of 3% (6%) in pp (p–Pb) collisions. A further contribution was added to account for the imperfect description of the material budget of the detector in the MC simulations, which especially affects the absorption of protons and thus the reconstruction efficiency. This was determined by comparing the corrected yields of charged pions, kaons, and protons using a standard MC production and one with the material budget increased

by 10%, which corresponds to a 2σ modification based on the estimated systematic uncertainty on the ALICE material budget [57]. The resulting uncertainty on the Λ_c^+ yield is 2% in the interval $0 < p_T < 1$ GeV/c, leading to an overall tracking efficiency uncertainty of 4% in pp collisions and 6% in p–Pb collisions.

The possible systematic uncertainty due to the dependence of the efficiencies on the generated p_T distribution of Λ_c^+ in the simulation was studied ("Monte Carlo p_T shape" in Table II). It was verified that the acceptance and the reconstruction efficiency do not significantly vary within the $0 < p_T < 1$ GeV/c interval. Following the same procedure as in Ref. [11], the efficiencies were evaluated after reweighting the p_T shape of the PYTHIA 8 simulations to match the p_T spectrum of D mesons from FONLL pQCD calculations [54,55], as no FONLL calculations exist for charm baryons. An uncertainty was assigned based on the difference between the nominal and reweighted efficiencies. No significant variation was observed in pp collisions, while a 1% variation was observed and assigned as systematic uncertainty in p–Pb collisions.

The systematic uncertainty on the feed-down subtraction was evaluated by considering the theoretical uncertainties of the beauty-meson production cross section in FONLL [54,55], and the variation of the beauty fragmentation function describing the hadronization $f(b \rightarrow \Lambda_b^0)$ within its uncertainties as measured in Ref. [23]. For p–Pb collisions a further consideration is made, varying the ratio of the feed-down and prompt Λ_c^+ nuclear modification factors $R_{p\mathrm{Pb}}^{\mathrm{feed\text{-}down}}/R_{p\mathrm{Pb}}^{\mathrm{prompt}}$ within the range 0.9–3.0. The upper bound of this range accounts for recent measurements by LHCb of the nuclear modification of Λ_b^0 baryons [58], where the nuclear modification factor at backward rapidity was found to be consistent with unity. The overall envelope from the variations was considered as the total uncertainty, resulting in $^{+0.9}_{-1.5}$% in pp collisions and $^{+0.9}_{-3.8}$% in p–Pb collisions.

The production cross section has an additional global normalization uncertainty due to the integrated luminosity determination. The luminosity uncertainty was determined from van der Meer scans of pp and p–Pb collisions at $\sqrt{s_{NN}} = 5.02$ TeV, and has a value of 2.1% for the pp data sample [46] and 3.7% for p–Pb collisions [47].

The 5% branching ratio uncertainty for the decay channel $\Lambda_c^+ \rightarrow pK_S^0(\rightarrow p\pi^+\pi^-)$ is calculated as the quadratic sum of the branching ratio uncertainties for $\Lambda_c^+ \rightarrow pK_S^0$ and $K_S^0 \rightarrow \pi^+\pi^-$ [48]. This uncertainty is considered as fully correlated between p_T intervals and collision systems.

VI. RESULTS

The p_T-differential Λ_c^+ production cross sections were calculated according to Eq. (1) and are shown in Fig. 3, where blue markers are used for pp collisions and black markers for p–Pb collisions. In each collision system, the new result in $0 < p_T < 1$ GeV/c is shown as an open marker, and the filled markers represent the previous measurements for $p_T > 1$ GeV/c from Refs. [11,12]. The Λ_c^+ production cross sections are compared with next-to-leading-order (NLO) pQCD calculations obtained with the POWHEG framework [59], matched with PYTHIA6 [61] to generate the parton shower
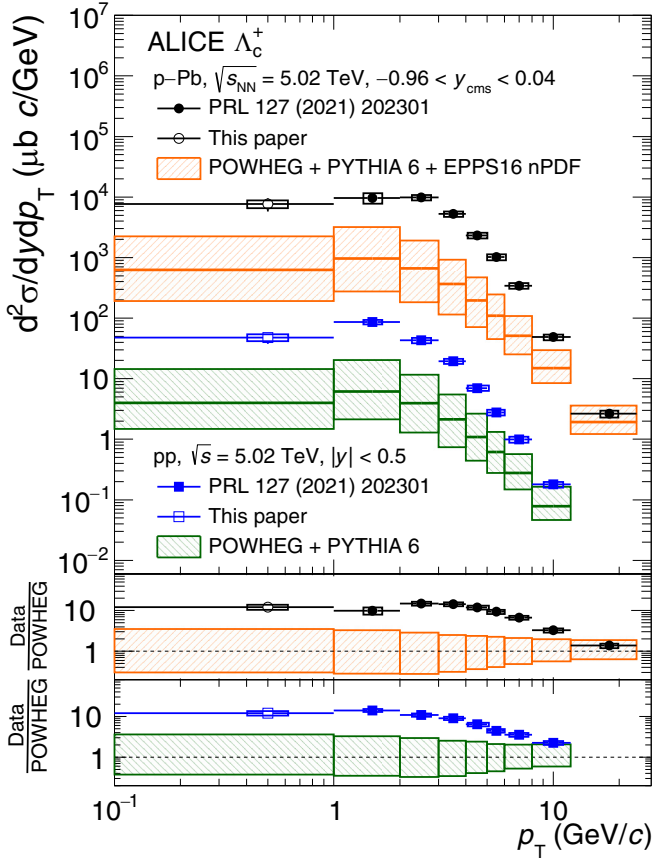
FIG. 3. The p_T-differential Λ_c^+ production cross sections in pp and p–Pb collisions at $\sqrt{s_{NN}} = 5.02$ TeV [12], including the new measurements in $0 < p_T < 1$ GeV/c as open markers. The lower panels show the ratios of the measurements to POWHEG+PYTHIA6, with EPPS16 nPDF calculations included for p–Pb collisions [9,59,60].

and fragmentation, and the CT14NLO parton distribution functions [62]. For p–Pb collisions, the nuclear modification of the parton distribution functions is modelled with the EPPS16 nuclear PDF (nPDF) parametrization [60]. The nominal factorization and renormalization scales, μ_F and μ_R, were taken to be equal to the transverse mass of the quark, $\mu_0 = \sqrt{m_c^2 + p_T^2}$, and the charm-quark mass was set to $m_c = 1.5$ GeV/c^2. The theoretical uncertainties were estimated by varying these scales in the range $0.5\mu_0 < \mu_{R,F} < 2.0\mu_0$, with the constraint $0.5 < \mu_R/\mu_F < 2.0$, as described in Ref. [54]. For the p–Pb case, the uncertainties on the parton distribu-

tion functions and EPPS16 nPDF are not included in the calculation as they are considerably smaller than the scale uncertainties. In both collision systems the measured p_T-differential production cross section values are significantly underestimated by the POWHEG predictions. In particular, in the interval $0 < p_T < 1$ GeV/c the model underestimates the measurements by a factor of about 10, similar to what was observed up to $p_T = 3$ GeV/c in Ref. [11].

The measured differential production cross sections in $0 < p_T < 1$ GeV/c are reported in Table III and compared with the values from Ref. [11], where the $0 < p_T < 1$ GeV/c region was determined from an extrapolation. For both pp and p–Pb collisions, the measured values are lower than the extrapolated ones and have smaller overall uncertainties, but remain within 1σ when considering the combined measurement and extrapolation uncertainties. The previously computed extrapolated production cross section in pp collisions was based on PYTHIA 8 predictions with specific tunes implementing color-reconnection mechanisms beyond the leading-color approximation, and the extrapolation uncertainty was assigned by taking the envelope of the different tunes. In p–Pb collisions, the extrapolation was performed by multiplying the extrapolated regions of the production cross section in pp collisions by i) the Pb mass number, ii) a correction factor to account for the different rapidity intervals covered in pp and p–Pb collisions, and iii) a factor based on an assumption on the nuclear modification factor $R_{p\mathrm{Pb}}$. The central value was calculated using $R_{p\mathrm{Pb}} = 0.5$ and the extrapolation uncertainty was estimated by varying this hypothesis in the range $0.35 < R_{p\mathrm{Pb}} < 0.8$ [11].

The production cross section measurement in the interval $0 < p_T < 1$ GeV/c allows the p_T-integrated production cross section to be calculated without the need for a model-dependent extrapolation, which in the previous publication [11] accounted for about 30% (20%) of the total Λ_c^+ production cross section in pp (p–Pb) collisions. The rapidity-differential production cross sections for $0 < p_T < 1$ GeV/c were summed with the values measured for the region $1 < p_T < 12$ (24) GeV/c for pp (p–Pb) collisions in Ref. [11] to obtain the integrated cross section. No extrapolation towards higher p_T is performed in either system, as the contribution to the p_T-integrated production cross section is negligible ($<0.1\%$) for the reported level of precision. The systematic uncertainties due to the raw-yield extraction were propagated as uncorrelated between p_T intervals, and all other sources were considered as fully correlated. The resulting p_T-integrated prompt Λ_c^+ production cross sections in the two collision systems are reported in Table IV, and compared with

TABLE III. The Λ_c^+ production cross sections at $0 < p_T < 1$ GeV/c in pp collisions for $|y| < 0.5$ and p–Pb collisions for $-0.96 < y_{\mathrm{cms}} < 0.04$, at $\sqrt{s_{NN}} = 5.02$ TeV. The left values are the new measurements from this article, and the right ones are the previously extrapolated values from Ref. [11].

	$d^2\sigma/dp_T dy$ ($0 < p_T < 1$ GeV/c)	
	Measured	Extrapolated [11]
pp (μb (GeV/c)$^{-1}$)	47.9 ± 10.4 (stat.) ± 6.1 (syst.) ± 1.0 (lumi.)	$68.5^{+11.9}_{-15.9}$ (extr.)
p–Pb (mb (GeV/c)$^{-1}$)	7.7 ± 1.9 (stat.) ± 1.1 (syst.) ± 0.3 (lumi.)	$8.5^{+5.1}_{-2.6}$ (extr.)

TABLE IV. The p_T-integrated production cross sections for prompt Λ_c^+ baryons in pp collisions for $|y| < 0.5$ and p–Pb collisions for $-0.96 < y_{cms} < 0.04$, at $\sqrt{s_{NN}} = 5.02$ TeV. The first two rows correspond to the measured values over the full p_T range, and the last two rows to the previously extrapolated results from Ref. [11].

	$d\sigma^{\Lambda_c^+}/dy$
pp, measured (μb)	208 ± 15 (stat.) ± 15 (syst.) ± 4 (lumi.)
p–Pb, measured (mb)	36.9 ± 3.3 (stat.) ± 4.5 (syst.) ± 1.4 (lumi.)
pp, extrapolated (μb) [11]	230 ± 16 (stat.) ± 20 (syst.) ± 5 (lumi.)$^{+5}_{-10}$ (extr.)
p–Pb, extrapolated (mb) [11]	36.2 ± 2.5 (stat.) ± 4.5 (syst.) ± 1.3 (lumi.)$^{+4.4}_{-2.7}$ (extr.)

the values published in Ref. [11] based on the p_T extrapolation described above.

The new measurement in the $0 < p_T < 1$ GeV/c interval in pp collisions results in a reduction of the p_T-integrated Λ_c^+ production cross section by about 10% with respect to the previous published results, but the two values remain compatible in terms of the combined statistical and systematic uncertainties. In p–Pb collisions the p_T-integrated Λ_c^+ production cross section is also compatible with the previous measurement [11].

In order to compare the spectral shapes in the two different collision systems at the same energy, the nuclear modification factor R_{pPb}, which is the ratio between the Λ_c^+ production cross sections in p–Pb and pp collisions, scaled by the nuclear mass number $A = 208$ and corrected to account for the shift in rapidity between pp and p–Pb collisions using FONLL [54], is calculated. The systematic uncertainties on the branching ratio and beauty feed-down are considered as fully correlated between the two collision systems, and all other systematic uncertainties as uncorrelated. This is shown as a function of p_T in Fig. 4. The R_{pPb} in $0 < p_T < 1$ GeV/c is consistent with unity within the uncertainties, and is also consistent

FIG. 4. Nuclear modification factor R_{pPb} of prompt Λ_c^+ baryons in p–Pb collisions at $\sqrt{s_{NN}} = 5.02$ TeV as a function of p_T, compared with model calculations [59,60,63,64].

with the decreasing trend towards low p_T within $0 < p_T < 6$ GeV/c that was previously observed in Ref. [11]. The results are compared with the POWHEG+PYTHIA6 [59,60] and POWLANG [63] models, as well as the QCM model [64]. In the QCM model, the charm quark is combined with a co-moving light antiquark or with two co-moving quarks to form a charm meson or baryon. For light-flavor (u, d, and s) quarks, the momentum distribution is obtained by fitting the data of hadronic p_T spectra using the quark coalescence formulas of QCM and parametrizing the hadron and quark spectra with a Lévy-Tsallis function, as explained in Ref. [65]. A free parameter, $R_{B/M}^{(c)}$, characterizes the relative production of single-charm baryons to single-charm mesons. This value is set to 0.425, which is tuned to reproduce the Λ_c^+/D^0 ratio measured by ALICE in pp collisions at $\sqrt{s} = 7$ TeV [10]. The relative abundances of the different charm-baryon species are determined by thermal weights from the statistical hadronization approach [66]. The POWHEG+PYTHIA6 pQCD event generator, which is coupled with the EPPS16 nPDF set for p–Pb collisions, predicts a central R_{pPb} value that is below unity for all p_T and constant for $p_T > 4$ GeV/c, but consistent with unity within the uncertainties. It should be noted that the uncertainties on this calculation come solely from the EPPS16 nPDF parametrization, as the uncertainties related to the pQCD scales in the POWHEG+PYTHIA6 calculation cancel out in the ratio between p–Pb and pp collisions. While the model is in fair agreement with the measurements for $p_T < 3$ GeV/c, it does not describe the increase above unity in the region $4 < p_T < 8$ GeV/c. Similarly, the POWLANG calculations are peaked in the region $2 < p_T < 4$ GeV/c, but are at tension with the data for $p_T > 4$ GeV/c. In the case of POWLANG, the R_{pPb} is the result of the transport of charm quarks through an expanding quark-gluon plasma, which is assumed to be formed in p–Pb collisions and affects the p_T distributions of charm hadrons. However, the calculated value is identical for all charm-hadron species as it does not consider any modifications of the relative hadron abundances due to quark coalescence. The QCM model, which does not include any nPDF or cold nuclear matter effects, gives the closest description of the measurement over the full measured p_T range.

The p_T-integrated R_{pPb} of prompt Λ_c^+ baryons was calculated from the p_T-integrated production cross sections measured in p–Pb and pp collisions, and is reported in Table V. The value is consistent with the atomic mass number scaling of the Λ_c^+ production cross section in pp collisions (i.e., $R_{pPb} = 1$), within 1.1σ of the combined statistical and systematic uncertainties. The p_T-integrated production cross
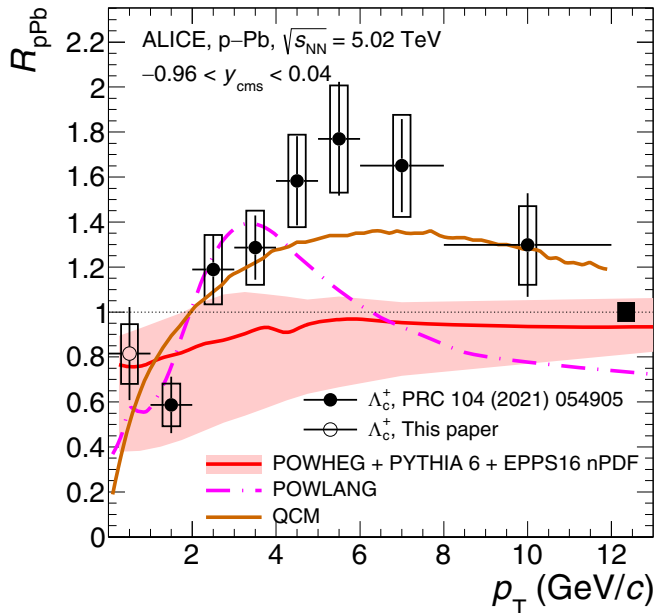
TABLE V. The p_T-integrated nuclear modification factors $R_{p\mathrm{Pb}}$ and R_{AA} of prompt Λ_c^+ baryons in p–Pb and Pb–Pb collisions at $\sqrt{s_{NN}} = 5.02$ TeV. The Pb–Pb results are derived from the integrated yields published in Ref. [35]. The percentile ranges in the first column represent the centrality ranges considered for Pb–Pb collisions.

	Λ_c^+ nuclear modification factor
p–Pb	0.85 ± 0.09 (stat.) ± 0.11 (syst.)
Pb–Pb (0–10%)	0.68 ± 0.10 (stat.) ± 0.10 (syst.)$^{+0.10}_{-0.06}$ (extr.)
Pb–Pb (30–50%)	0.86 ± 0.13 (stat.) ± 0.13 (syst.)$^{+0.09}_{-0.06}$ (extr.)

section in pp collisions from Table IV is also used to compute the R_{AA} of prompt Λ_c^+ baryons from the p_T-integrated corrected yields in central (0–10%) and semicentral (30–50%) Pb–Pb collisions at $\sqrt{s_{NN}} = 5.02$ TeV reported in Ref. [35]. These values are also reported in Table V. The extrapolation uncertainties on the Pb–Pb nuclear modification factors arise due to the extrapolation of the Pb–Pb Λ_c^+-baryon yields down to $p_T = 0$, which was performed by estimating the Λ_c^+/D^0 ratio in $0 < p_T < 1$ GeV/c with model calculations [32,67–69] and multiplying it by the measured D^0-meson yield [70]. The uncertainty was determined from the variation of the resulting Λ_c^+ yield with different model calculations.

Figure 5 shows the p_T-integrated nuclear modification factors for Λ_c^+ baryons in p–Pb and Pb–Pb collisions, compared with those measured for D^0 mesons in Ref. [70]. The p_T-integrated R_{AA} of Λ_c^+ is 1.8σ below unity in 0–10% central collisions, indicating a suppression of the Λ_c^+-baryon yield in Pb–Pb collisions with respect to the binary-scaled pp reference due to shadowing and possible modifications in the

FIG. 5. The p_T-integrated nuclear modification factors of prompt Λ_c^+ baryons and D^0 mesons measured in p–Pb and Pb-Pb collisions at $\sqrt{s_{NN}} = 5.02$ TeV [35,70]. Statistical (bars) and systematic and extrapolation (brackets) uncertainties are shown. The measurements are compared with calculations from the theoretical models nCTEQ15 [71–73] and EPPS16 [60] that include only initial-state effects. The uncertainty bands on the models represent the 90% confidence level.

hadronization mechanism. In the 30–50% centrality interval, the p_T-integrated Λ_c^+ R_{AA} is compatible with unity within the uncertainties. The p_T-integrated Λ_c^+ $R_{p\mathrm{Pb}}$ is closer to unity than the R_{AA} in central Pb–Pb collisions, as expected from the smaller shadowing effects in p–Pb compared to Pb–Pb collisions, where the nucleons of both the projectile and the target nuclei are involved. In all three collision systems, the nuclear modification factors for Λ_c^+ and D^0 are consistent with one another, indicating that there is no significant enhancement of the overall production of charm baryons compared to charm mesons in heavy-ion collisions. The integrated R_{AA} and $R_{p\mathrm{Pb}}$ are also compared with perturbative QCD calculations including only initial-state effects modeled using two different sets of nuclear PDFs, namely a Bayesian-reweighted version [71,72] of nCTEQ15 [73] and EPPS16 [60]. The calculations with EPPS16 do not include the dependence of the shadowing on the impact parameter of the Pb–Pb collision, and therefore they are identical in the central and semicentral event classes. The predictions with nCTEQ15 are obtained by applying a Bayesian reweighting of the nuclear PDFs, which is constrained by measurements of heavy-flavor hadron production in p–Pb collisions at the LHC [71], and are labeled as nCTEQ15$_{\mathrm{rwHF}}$ in Fig. 5. The uncertainty bands for both calculations represent the 90% confidence level regions. In the reweighted nCTEQ15 case they are determined by considering three different factorization scales in addition to the PDF uncertainties. The measured R_{AA} and $R_{p\mathrm{Pb}}$ values are within the upper edge of the nCTEQ15 uncertainty band. These data provide an important input for testing the assumptions of nPDFs in theoretical calculations.

The Λ_c^+/D^0 baryon-to-meson yield ratio is used to further examine differences in the charm-quark hadronization into baryons and mesons that may arise due to the differing numbers of constituent quarks. The results in pp and p–Pb collisions are shown in the left panel of Fig. 6. The p_T-differential D^0 production cross section in $0 < p_T < 1$ GeV/c was taken from Ref. [3] for pp collisions and from Ref. [26] for p–Pb collisions. In the calculation of the baryon-to-meson ratio, the uncertainties related to the tracking efficiency, luminosity, and beauty feed-down were treated as fully correlated between the two species, and all other uncertainty contributions were considered to be uncorrelated. The Λ_c^+/D^0 yield ratio in $0 < p_T < 1$ GeV/c in both pp and p–Pb collisions indicates a decreasing trend with respect to the intermediate p_T region, albeit with large uncertainties. Within uncertainties, the Λ_c^+/D^0 ratios are consistent between pp and p–Pb collisions. The distribution has a maximum in the region $1 < p_T < 3$ ($3 < p_T < 5$) GeV/c in pp (p–Pb) collisions. The shift of the peak towards higher p_T in p–Pb collisions could be attributed to a contribution of collective effects, e.g., radial flow. Similar collective effects have been observed for light- and heavy-flavor hadrons in p–Pb collisions at the LHC [75–77]. Such a contribution would be consistent with previous observations for the light-flavor Λ/K_S^0 baryon-to-meson ratio [29]. The results are also compared with the QCM model [20,74] which describes the magnitude of the Λ_c^+/D^0 ratio well for $0 < p_T < 12$ GeV/c in both collision systems, as well as predicting a shift of the peak towards higher p_T, resulting from a hardening of the Λ_c^+ spectrum in p–Pb collisions.
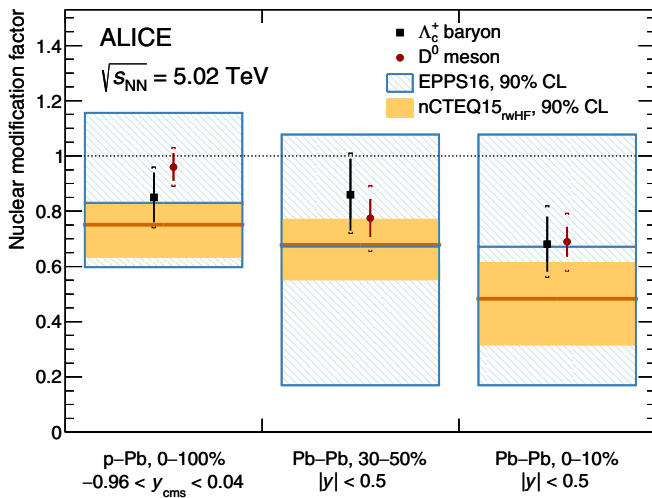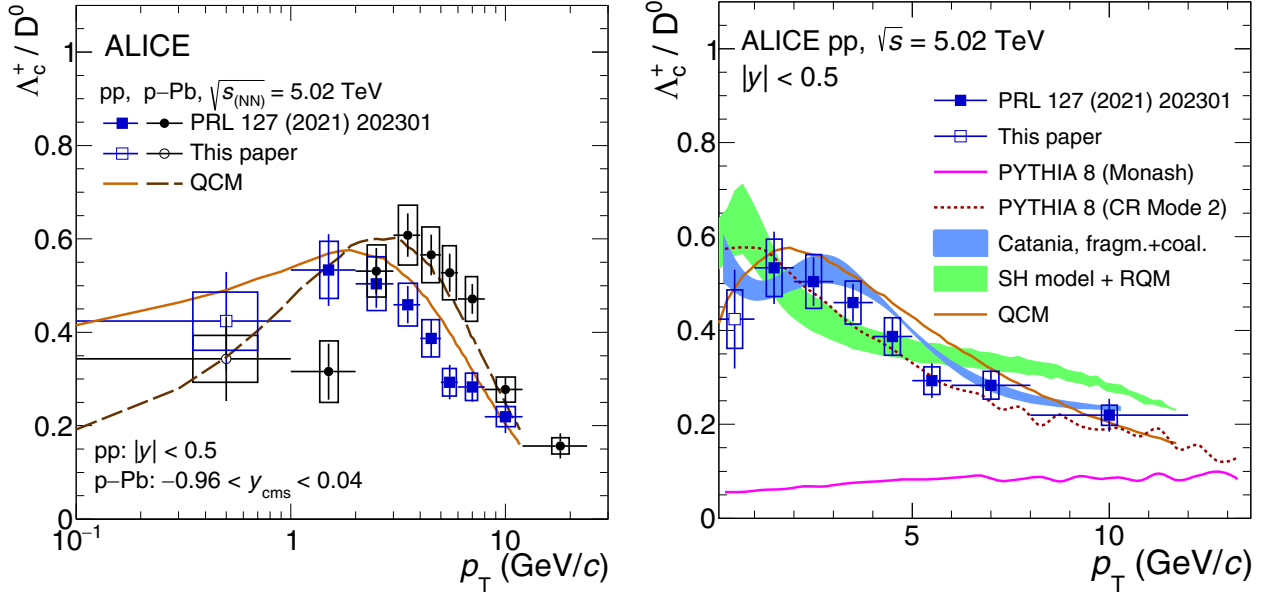
FIG. 6. Left: Λ_c^+/D^0 ratio in pp and p–Pb collisions as a function of p_T, compared with the QCM model [64,74]. Right: Λ_c^+/D^0 ratio as a function of p_T in pp collisions at $\sqrt{s} = 5.02$ TeV, including comparisons with models [9,18,19,21,74].

The modification of the Λ_c^+-baryon production spectrum in p–Pb collisions is confirmed by computing the mean transverse momentum, $\langle p_T \rangle$. This was calculated in each collision system following the same prescription as in Ref. [56], with the central value derived from a power-law fit to the p_T spectrum. The resulting values are summarized in Table VI and compared with the values obtained for D^0 mesons in Ref. [26]. The $\langle p_T \rangle$ value for Λ_c^+ baryons is significantly higher in p–Pb collisions than in pp collisions, by 3.7σ considering the combined statistical and systematic uncertainties. This is in contrast with the results for D^0 mesons, for which the $\langle p_T \rangle$ is seen to be fully consistent between the two collision systems.

The right panel of Fig. 6 shows the Λ_c^+/D^0 yield ratio in pp collisions as a function of p_T compared with model calculations in which different hadronization processes are implemented. The Monash tune of PYTHIA 8 [9], which implements fragmentation processes tuned on charm-hadron production measurements in e^+e^- collisions, predicts an integrated value of about 0.1 for the Λ_c^+/D^0 ratio, with a mild p_T dependence. This significantly underpredicts the data, as already seen in Refs. [11,12], with a difference of approximately a factor 8 between the data and model in the interval $0 < p_T < 1$ GeV/c. Model calculations including processes that enhance baryon production, like PYTHIA 8 including color reconnection beyond the leading-color approximation

[18], SHM+RQM [21], QCM [74], and Catania [19] are also shown. Hadronization in PYTHIA 8 is built on the Lund string fragmentation model [78], where quarks and gluons connected by color strings fragment into hadrons, and color reconnection allows for partons created in the collision to interact via color strings. The tune with color-reconnection topologies beyond the leading-color approximation includes so-called "junctions" that fragment into baryons and lead to increased baryon production with respect to the Monash tune. The statistical hadronization model includes additional excited charm-baryon states that have not yet been observed but are predicted by the relativistic quark model [79]. These additional states decay strongly to Λ_c^+ baryons, thereby contributing to the prompt Λ_c^+ spectrum. The SHM+RQM predictions include a source of uncertainty related to the branching ratios of the excited baryon states into Λ_c^+ final states, which is estimated by varying the branching ratios between 50% and 100%. The Catania model assumes that a color-deconfined state of matter is formed in pp collisions, and hadronization can occur via quark coalescence in addition to fragmentation. Coalescence is implemented through the Wigner formalism, where a blast-wave model is used to determine the p_T spectrum of light quarks, and FONLL pQCD calculations are used for heavy quarks. Hadronization via coalescence is predicted to dominate at low p_T, while

TABLE VI. Mean transverse momentum values for D^0 mesons [26] and Λ_c^+ baryons in pp and p–Pb collisions at $\sqrt{s_{NN}} = 5.02$ TeV.

	$\langle p_T \rangle$ (GeV/c)	
	pp	*p*–Pb
D^0	2.06 ± 0.03 (stat.) ± 0.03 (syst.)	2.07 ± 0.02 (stat.) ± 0.04 (syst.)
Λ_c^+	1.86 ± 0.06 (stat.) ± 0.03 (syst.)	2.29 ± 0.06 (stat.) ± 0.06 (syst.)

TABLE VII. The p_T-integrated Λ_c^+/D^0 yield ratios in pp and p–Pb collisions at $\sqrt{s_{NN}} = 5.02$ TeV.

	Λ_c^+/D^0
pp	0.47 ± 0.04 (stat.) ± 0.04 (syst.)
p–Pb	0.42 ± 0.04 (stat.) ± 0.06 (syst.)

fragmentation dominates at high p_T. All of these models qualitatively reproduce the data. The QCM model predicts a maximum in the region $1 < p_T < 3$ GeV/c, while the other models tend to predict a continuous increase of the Λ_c^+/D^0 yield ratio towards low p_T, reaching a value of about 0.6 at $p_T = 0$. This trend might highlight some tension with the data in the interval $0 < p_T < 1$ GeV/c, since the data hint to a decrease of the Λ_c^+/D^0 yield ratio, though a more precise measurement is needed to reach a firm conclusion.

The p_T-integrated Λ_c^+/D^0 yield ratios in pp and p–Pb collisions are presented in Table VII. These are consistent with each other within 1σ of the combined statistical and systematic uncertainties, indicating no modification of the overall hadronization fractions between pp and p–Pb collisions despite the modification of the $\langle p_T \rangle$. A similar effect was observed for Λ_c^+ baryons measured as a function of charged-particle multiplicity in pp collisions at $\sqrt{s} = 13$ TeV [27], where the p_T-integrated Λ_c^+/D^0 ratio was found to be independent of multiplicity despite a significant alteration of the p_T-dependent spectrum. This could indicate a common mechanism that alters the p_T distribution of charm baryons for p–Pb and high-multiplicity pp collisions while leaving the integrated relative abundance of baryons and mesons consistent with lower-multiplicity pp collisions.

VII. SUMMARY

The first measurements of the production of prompt Λ_c^+ baryons in the transverse momentum interval $0 < p_T < 1$ GeV/c in pp ($|y| < 0.5$) and in p–Pb ($-0.96 < y_{cms} < 0.04$) collisions at $\sqrt{s_{NN}} = 5.02$ TeV with the ALICE detector at the LHC are reported, removing the model dependence affecting the previous results for the p_T-integrated Λ_c^+ yields [11]. The analysis was performed using the decay channel $\Lambda_c^+ \to pK_S^0$. The Λ_c^+ production cross section in the interval $0 < p_T < 1$ GeV/c was measured to be larger than predictions given by pQCD-based calculations in both pp and p–Pb collisions. The uncertainties on the two measurements are smaller than the theoretical uncertainties on the previously extrapolated values [11]. The p_T-differential $R_{p\text{Pb}}$ was measured in $0 < p_T < 1$ GeV/c and found to be consistent with unity within the uncertainties, and also with a decreasing trend towards low p_T in $0 < p_T < 6$ GeV/c. However, the current precision of the measurement is not enough to draw firm conclusions on the role of cold nuclear matter effects and on the possible presence of collective effects, like the radial flow, which are observed in heavy-ion collisions. In addition, the p_T-integrated $R_{p\text{Pb}}$ and R_{AA} of prompt Λ_c^+ baryons were obtained and compared with those of D^0 mesons at the same center-of-mass energy, showing compatibility between the nuclear modification factors of

the two charm hadron species. The results are consistent with calculations that consider nuclear modification of the PDFs.

The Λ_c^+/D^0 yield ratio in $0 < p_T < 1$ GeV/c in both pp and p–Pb collisions indicates a decreasing trend with respect to the intermediate p_T region, albeit with large uncertainties. The PYTHIA 8 event generator with the Monash tune, which incorporates fragmentation parameters from e^+e^- collisions, significantly underestimates the Λ_c^+/D^0 yield ratio. The data are qualitatively reproduced by models that predict an enhancement of baryon production by various mechanisms, including color reconnection beyond the leading-color approximation, feed-down from unobserved resonant charm-baryon states, or quark coalescence (recombination). The quark (re)combination model also describes the shift of the peak in the Λ_c^+/D^0 ratio between pp and p–Pb collisions. The hardening of the p_T spectrum of Λ_c^+ baryons is confirmed by calculating the $\langle p_T \rangle$, resulting in a 3.7σ modification between pp and p–Pb collisions. The measurement of the Λ_c^+ baryon in the interval $0 < p_T < 1$ GeV/c in pp and p–Pb collisions and the p_T-integrated results are crucial for providing further insight into charm-quark hadronization in pp and p–Pb collisions, and for the investigation of cold nuclear matter effects in p–Pb collisions. More precise measurements are expected to be performed during Runs 3 and 4 of the LHC thanks to the upgraded ALICE detector [80].

[1] J. C. Collins, D. E. Soper, and G. F. Sterman, Factorization of hard processes in QCD, Adv. Ser. Direct. High Energy Phys. **5**, 1 (1989).

[2] M. Cacciari, M. Greco, and P. Nason, The p_T spectrum in heavy flavor hadroproduction, J. High Energy Phys. 05 (1998) 007.

[3] S. Acharya *et al.* (ALICE Collaboration), Measurement of beauty and charm production in *pp* collisions at $\sqrt{s} = 5.02$ TeV via non-prompt and prompt D mesons, J. High Energy Phys. 05 (2021) 220.

[4] S. Acharya *et al.* (ALICE Collaboration), Measurement of D-meson production at mid-rapidity in *pp* collisions at $\sqrt{s} = 7$ TeV, Eur. Phys. J. C **77**, 550 (2017).

[5] R. Aaij *et al.* (LHCb Collaboration), Measurements of prompt charm production cross-sections in *pp* collisions at $\sqrt{s} = 5$ TeV, J. High Energy Phys. 06 (2017) 147.

[6] A. Tumasyan *et al.* (CMS Collaboration), Measurement of prompt open-charm production cross sections in proton–proton collisions at $\sqrt{s} = 13$ TeV, J. High Energy Phys. 11 (2021) 225.

[7] L. Gladilin, Fragmentation fractions of *c* and *b* quarks into charmed hadrons at LEP, Eur. Phys. J. C **75**, 19 (2015).

[8] T. Sjöstrand, S. Mrenna, and P. Skands, A brief introduction to PYTHIA 8.1, Comput. Phys. Commun. **178**, 852 (2008).

[9] P. Skands, S. Carrazza, and J. Rojo, Tuning PYTHIA 8.1: The Monash 2013 tune, Eur. Phys. J. C **74**, 3024 (2014).

[10] S. Acharya *et al.* (ALICE Collaboration), Λ_c^+ production in *pp* collisions at $\sqrt{s} = 7$ TeV and in p–Pb collisions at $\sqrt{s_{NN}} = 5.02$ TeV, J. High Energy Phys. 04 (2018) 108.

[11] S. Acharya *et al.* (ALICE Collaboration), Λ_c^+ production in *pp* and in *p*–Pb collisions at $\sqrt{s_{NN}} = 5.02$ TeV, Phys. Rev. C **104**, 054905 (2021).

[12] S. Acharya *et al.* (ALICE Collaboration), Λ_c^+ Production and Baryon-to-Meson Ratios in *pp* and p–Pb Collisions at $\sqrt{s_{NN}} = 5.02$ TeV at the LHC, Phys. Rev. Lett. **127**, 202301 (2021).

[13] A. M. Sirunyan *et al.* (CMS Collaboration), Production of Λ_c^+ baryons in proton-proton and lead-lead collisions at $\sqrt{s_{NN}} = 5.02$ TeV, Phys. Lett. B **803**, 135328 (2020).

[14] S. Acharya *et al.* (ALICE Collaboration), Measurement of the production cross section of prompt Ξ_c^0 baryons at midrapidity in *pp* collisions at $\sqrt{s} = 5.02$ TeV, J. High Energy Phys. 10 (2021) 159.

[15] S. Acharya *et al.* (ALICE Collaboration), Measurement of the Cross Sections of Ξ_c^0 and Ξ_c^+ Baryons and of the Branching-Fraction Ratio BR($\Xi_c^0 \to \Xi^- e^+ \nu_e$)/BR($\Xi_c^0 \to \Xi^- \pi^+$) in *pp* Collisions at 13 TeV, Phys. Rev. Lett. **127**, 272001 (2021).

[16] S. Acharya *et al.* (ALICE Collaboration), Measurement of Prompt D^0, Λ_c^+, and $\Sigma_c^{0,++}$(2455) Production in Proton–Proton Collisions at $\sqrt{s} = 13$ TeV, Phys. Rev. Lett. **128**, 012001 (2022).

[17] S. Acharya *et al.* (ALICE Collaboration), First measurement of Ω_c^0 production in *pp* collisions at $\sqrt{s} = 13$ TeV, arXiv:2205.13993 [nucl-ex].

[18] J. R. Christiansen and P. Z. Skands, String formation beyond leading colour, J. High Energy Phys. 08 (2015) 003.

[19] V. Minissale, S. Plumari, and V. Greco, Charm hadrons in *pp* collisions at LHC energy within a coalescence plus fragmentation approach, Phys. Lett. B **821**, 136622 (2021).

[20] J. Song, H.-h. Li, and F.-l. Shao, New feature of low p_T charm quark hadronization in *pp* collisions at $\sqrt{s} = 7$ TeV, Eur. Phys. J. C **78**, 344 (2018).

[21] M. He and R. Rapp, Charm-baryon production in proton-proton collisions, Phys. Lett. B **795**, 117 (2019).

[22] S. Chatrchyan *et al.* (CMS Collaboration), Measurement of the Λ_b cross section and the $\bar{\Lambda}_b$ to Λ_b ratio with $J/\Psi\Lambda$ decays in *pp* collisions at $\sqrt{s} = 7$ TeV, Phys. Lett. B **714**, 136 (2012).

[23] R. Aaij *et al.* (LHCb Collaboration), Measurement of b hadron fractions in 13 TeV *pp* collisions, Phys. Rev. D **100**, 031102 (2019).

[24] R. Aaij *et al.* (LHCb Collaboration), Study of the production of Λ_b^0 and $\overline{B}^0$ hadrons in *pp* collisions and first measurement of the $\Lambda_b^0 \to J/\psi pK^-$ branching fraction, Chin. Phys. C **40**, 011001 (2016).

[25] S. Acharya *et al.* (ALICE Collaboration), Charm-quark fragmentation fractions and production cross section at midrapidity in *pp* collisions at the LHC, Phys. Rev. D **105**, L011103 (2022).

[26] S. Acharya *et al.* (ALICE Collaboration), Measurement of prompt D^0, D^+, D^{*+}, and D_s^+ production in p–Pb collisions at $\sqrt{s_{NN}} = 5.02$ TeV, J. High Energy Phys. 12 (2019) 092.

[27] S. Acharya *et al.* (ALICE Collaboration), Observation of a multiplicity dependence in the p_T-differential charm baryon-to-meson ratios in proton–proton collisions at $\sqrt{s} = 13$ TeV, Phys. Lett. B **829**, 137065 (2022).

[28] LHCb Collaboration, "Measurement of the Λ_c^+ to D^0 production cross-section ratio in peripheral PbPb collisions, arXiv:2210.06939 [hep-ex].

[29] B. B. Abelev *et al.* (ALICE Collaboration), Multiplicity dependence of pion, kaon, proton and Lambda production in p–Pb collisions at $\sqrt{s_{NN}} = 5.02$ TeV, Phys. Lett. B **728**, 25 (2014).

[30] A. M. Sirunyan *et al.* (CMS Collaboration), Strange hadron production in *pp* and pPb collisions at $\sqrt{s_{NN}} = 5.02$ TeV, Phys. Rev. C **101**, 064906 (2020).

[31] T. Pierog, I. Karpenko, J. M. Katzy, E. Yatsenko, and K. Werner, EPOS LHC: Test of collective hadronization with data measured at the CERN Large Hadron Collider, Phys. Rev. C **92**, 034906 (2015).

[32] E. Schnedermann, J. Sollfrank, and U. Heinz, Thermal phenomenology of hadrons from 200-AGeV S+S collisions, Phys. Rev. C **48**, 2462 (1993).

[33] R. J. Fries, B. Müller, C. Nonaka, and S. A. Bass, Hadronization in Heavy-Ion Collisions: Recombination and Fragmentation of Partons, Phys. Rev. Lett. **90**, 202303 (2003).

[34] N. Armesto, Nuclear shadowing, J. Phys. G **32**, R367 (2006).

[35] S. Acharya *et al.* (ALICE Collaboration), Constraining hadronization mechanisms with Λ_c^+/D^0 production ratios in Pb–Pb collisions at $\sqrt{s_{NN}} = 5.02$ TeV, Phys. Lett. B **839**, 137796 (2023).

[36] I. Kisel, I. Kulakov, and M. Zyzak, Standalone first level event selection package for the CBM Experiment, IEEE Trans. Nucl. Sci. **60**, 3703 (2013).

[37] T. Chen and C. Guestrin, XGBoost: A scalable tree boosting system, in *KDD '16: Proceedings of the 22nd ACM SIGKDD International Conference on Knowledge Discovery and Data Mining* (ACM, 2016), pp. 785–794.

[38] K. Aamodt *et al.* (ALICE Collaboration), The ALICE experiment at the CERN LHC, JINST **3**, S08002 (2008).

[39] B. B. Abelev *et al.* (ALICE Collaboration), Performance of the ALICE experiment at the CERN LHC, Int. J. Mod. Phys. A **29**, 1430044 (2014).

[40] K. Aamodt *et al.* (ALICE Collaboration), Alignment of the ALICE inner tracking system with cosmic-ray tracks, JINST **5**, P03003 (2010).

[41] J. Alme *et al.*, The ALICE TPC, a large 3-dimensional tracking device with fast readout for ultra-high multiplicity events, Nucl. Instrum. Methods Phys. Res. A **622**, 316 (2010).

[42] A. Akindinov *et al.*, Performance of the ALICE time-of-flight detector at the LHC, Eur. Phys. J. Plus **128**, 44 (2013).

[43] E. Abbas *et al.* (ALICE Collaboration), Performance of the ALICE VZERO system, JINST **8**, P10016 (2013).

[44] J. Adam *et al.* (ALICE Collaboration), Determination of the event collision time with the ALICE detector at the LHC, Eur. Phys. J. Plus **132**, 99 (2017).

[45] S. Acharya *et al.* (ALICE Collaboration), Pseudorapidity distributions of charged particles as a function of mid- and forward rapidity multiplicities in *pp* collisions at $\sqrt{s} = 5.02$, 7 and 13 TeV, Eur. Phys. J. C **81**, 630 (2021).

[46] S. Acharya *et al.* (ALICE Collaboration), ALICE 2017 luminosity determination for *pp* collisions at $\sqrt{s} = 5$ TeV, (Nov, 2018) ALICE–PUBLIC–2018–014. http://cds.cern.ch/record/2648933.

[47] B. Abelev *et al.* (ALICE Collaboration), Measurement of visible cross sections in proton–lead collisions at $\sqrt{s_{NN}} = 5.02$ TeV in van der Meer scans with the ALICE detector, JINST **9**, P11003 (2014).

[48] R. L. Workman *et al.* (Particle Data Group), Review of particle physics, Prog. Theor. Exp. Phys. **2022**, 083C01 (2022).

[49] L. Barioglio, F. Catalano, M. Concas, P. Fecchio, F. Grosa, F. Mazzaschi, and M. Puccio, hipe4ml/hipe4ml, Nov. 2021. https://doi.org/10.5281/zenodo.5734093.

[50] R. Brun *et al.*, GEANT: Detector Description and Simulation Tool; Oct 1994. CERN Program Library. CERN, Geneva, 1993, http://cds.cern.ch/record/1082634. Long Writeup W5013.

[51] X.-N. Wang and M. Gyulassy, HIJING: A Monte Carlo model for multiple jet production in pp, pA, and AA collisions, Phys. Rev. D **44**, 3501 (1991).

[52] T. Hastie, R. Tibshirani, and J. Friedman, *The Elements of Statistical Learning: Data Mining, Inference and Prediction*, 2nd ed. (Springer, New York, 2009), http://www-stat.stanford.edu/~tibs/ElemStatLearn/.

[53] S. M. Lundberg *et al.*, From local explanations to global understanding with explainable AI for trees, Nat. Mach. Intell. **2**, 56 (2020).

[54] M. Cacciari, S. Frixione, N. Houdeau, M. L. Mangano, P. Nason, and G. Ridolfi, Theoretical predictions for charm and bottom production at the LHC, J. High Energy Phys. 10 (2012) 137.

[55] M. Cacciari, M. L. Mangano, and P. Nason, Gluon PDF constraints from the ratio of forward heavy-quark production at the LHC at $\sqrt{s} = 7$ and 13 TeV, Eur. Phys. J. C **75**, 610 (2015).

[56] J. Adam *et al.* (ALICE Collaboration), D-meson production in p–Pb collisions at $\sqrt{s_{NN}} = 5.02$ TeV and in *pp* collisions at $\sqrt{s} = 7$ TeV, Phys. Rev. C **94**, 054908 (2016).

[57] B. Abelev *et al.* (ALICE Collaboration), Neutral pion and η meson production in proton–proton collisions at $\sqrt{s} = 0.9$ TeV and $\sqrt{s} = 7$ TeV, Phys. Lett. B **717**, 162 (2012).

[58] R. Aaij *et al.* (LHCb Collaboration), Measurement of B^+, B^0 and Λ_b^0 production in pPb collisions at $\sqrt{s_{NN}} = 8.16$ TeV, Phys. Rev. D **99**, 052011 (2019).

[59] S. Frixione, P. Nason, and G. Ridolfi, A Positive-weight next-to-leading-order Monte Carlo for heavy flavour hadroproduction, J. High Energy Phys. 09 (2007) 126.

[60] K. J. Eskola, P. Paakkinen, H. Paukkunen, and C. A. Salgado, EPPS16: Nuclear parton distributions with LHC data, Eur. Phys. J. C **77**, 163 (2017).

[61] T. Sjöstrand, S. Mrenna, and P. Skands, Pythia 6.4 physics and manual, J. High Energy Phys. 05 (2006) 026.

[62] S. Dulat *et al.*, New parton distribution functions from a global analysis of quantum chromodynamics, Phys. Rev. D **93**, 033006 (2016).

[63] A. Beraudo, A. De Pace, M. Monteno, M. Nardi, and F. Prino, Heavy-flavour production in high-energy d-Au and p–Pb collisions, J. High Energy Phys. 03 (2016) 123.

[64] H.-h. Li, F.-L. Shao, J. Song, and R.-q. Wang, Production of single-charm hadrons by quark combination mechanism in p-Pb collisions at $\sqrt{s_{NN}} = 5.02$ TeV, Phys. Rev. C **97**, 064915 (2018).

[65] X.-R. Gou, F.-L. Shao, R.-Q. Wang, H.-H. Li, and J. Song, New insights into hadron production mechanism from p_T spectra in pp collisions at $\sqrt{s} = 7$ TeV, Phys. Rev. D **96**, 094010 (2017).

[66] A. Andronic, F. Beutler, P. Braun-Munzinger, K. Redlich, and J. Stachel, Statistical hadronization of heavy flavor quarks in elementary collisions: Successes and failures, Phys. Lett. B **678**, 350 (2009).

[67] S. Plumari, V. Minissale, S. K. Das, G. Coci, and V. Greco, Charmed Hadrons from Coalescence plus Fragmentation in relativistic nucleus-nucleus collisions at RHIC and LHC, Eur. Phys. J. C **78**, 348 (2018).

[68] M. He and R. Rapp, Hadronization and Charm-Hadron Ratios in Heavy-Ion Collisions, Phys. Rev. Lett. **124**, 042301 (2020).

[69] A. Andronic, P. Braun-Munzinger, M. K. Köhler, A. Mazeliauskas, K. Redlich, J. Stachel, and V. Vislavicius, The multiple-charm hierarchy in the statistical hadronization model, J. High Energy Phys. 07 (2021) 035.

[70] S. Acharya *et al.* (ALICE Collaboration), Prompt D^0, D^+, and D^{*+} production in Pb–Pb collisions at $\sqrt{s_{NN}} = 5.02$ TeV, J. High Energy Phys. 01 (2022) 174.

[71] A. Kusina, J.-P. Lansberg, I. Schienbein, and H.-S. Shao, Gluon Shadowing in Heavy-Flavor Production at the LHC, Phys. Rev. Lett. **121**, 052004 (2018).

[72] A. Kusina, J.-P. Lansberg, I. Schienbein, and H.-S. Shao, Reweighted nuclear PDFs using heavy-flavor production data at the LHC, Phys. Rev. D **104**, 014010 (2021).

[73] K. Kovařík *et al.*, nCTEQ15 - Global analysis of nuclear parton distributions with uncertainties in the CTEQ framework, Phys. Rev. D **93**, 085037 (2016).

[74] H. Li, F. Shao, and J. Song, Production of light-flavor and single-charmed hadrons in pp collisions at $\sqrt{s} = 5.02$ TeV in an equal-velocity quark combination model, Chin. Phys. C **45**, 113105 (2021).

[75] V. Khachatryan *et al.* (CMS Collaboration), Long-range two-particle correlations of strange hadrons with charged particles in pPb and PbPb collisions at LHC energies, Phys. Lett. B **742**, 200 (2015).

[76] M. Aaboud *et al.* (ATLAS Collaboration), Measurements of long-range azimuthal anisotropies and associated Fourier coefficients for pp collisions at $\sqrt{s} = 5.02$ and 13 TeV and p+Pb collisions at $\sqrt{s_{NN}} = 5.02$ TeV with the ATLAS detector, Phys. Rev. C **96**, 024908 (2017).

[77] S. Acharya *et al.* (ALICE Collaboration), Azimuthal Anisotropy of Heavy-Flavor Decay Electrons in p-Pb Collisions at $\sqrt{s_{NN}} = 5.02$ TeV, Phys. Rev. Lett. **122**, 072301 (2019).

[78] B. Andersson, G. Gustafson, G. Ingelman, and T. Sjöstrand, Parton fragmentation and string dynamics, Phys. Rep. **97**, 31 (1983).

[79] D. Ebert, R. N. Faustov, and V. O. Galkin, Spectroscopy and Regge trajectories of heavy baryons in the relativistic quark-diquark picture, Phys. Rev. D **84**, 014025 (2011).

[80] B. Abelev *et al.* (ALICE Collaboration), Upgrade of the ALICE experiment: Letter of intent, J. Phys. G **41**, 087001 (2014).

S. Acharya [125] D. Adamová [86] A. Adler,[69] G. Aglieri Rinella [32] M. Agnello [29] N. Agrawal [50] Z. Ahammed [132] S. Ahmad [15] S. U. Ahn [70] I. Ahuja [37] A. Akindinov [140] M. Al-Turany [97] D. Aleksandrov [140] B. Alessandro [55] H. M. Alfanda [6] R. Alfaro Molina [66] B. Ali [15] A. Alici [25] N. Alizadehvandchali [114] A. Alkin [32] J. Alme [20] G. Alocco [51] T. Alt [63] I. Altsybeev [140] M. N. Anaam [6] C. Andrei [45] A. Andronic [135] V. Anguelov [94] F. Antinori [53] P. Antonioli [50] N. Apadula [74] L. Aphecetche [103] H. Appelshäuser [63] C. Arata [73] S. Arcelli [25] M. Aresti [51] R. Arnaldi [55] J. G. M. C. A. Arneiro [110] I. C. Arsene [19] M. Arslandok [137] A. Augustinus [32] R. Averbeck [97] M. D. Azmi [15] A. Badalà [52] J. Bae [104] Y. W. Baek [40] X. Bai [118] R. Bailhache [63] Y. Bailung [47] A. Balbino [29] A. Baldisseri [128] B. Balis [2] D. Banerjee [4] Z. Banoo [91] R. Barbera [26] F. Barile [31] L. Barioglio [95] M. Barlou,[78] G. G. Barnaföldi [136] L. S. Barnby [85] V. Barret [125] L. Barreto [110] C. Bartels [117] K. Barth [32] E. Bartsch [63] N. Bastid [125] S. Basu [75] G. Batigne [103] D. Battistini [95] B. Batyunya [141] D. Bauri,[46] J. L. Bazo Alba [101] I. G. Bearden [83] C. Beattie [137] P. Becht [97] D. Behera [47] I. Belikov [127] A. D. C. Bell Hechavarria [135] F. Bellini [25] R. Bellwied [114] S. Belokurova [140] V. Belyaev [140] G. Bencedi [136] S. Beole [24] A. Bercuci [45] Y. Berdnikov [140] A. Berdnikova [94] L. Bergmann [94] M. G. Besoiu [62] L. Betev [32] P. P. Bhaduri [132] A. Bhasin [91] M. A. Bhat [4] B. Bhattacharjee [41] L. Bianchi [24] N. Bianchi [48] J. Bielčík [35] J. Bielčíková [86] J. Biernat [107] A. P. Bigot [127] A. Bilandzic [95] G. Biro [136] S. Biswas [4] N. Bize [103] J. T. Blair [108] D. Blau [140] M. B. Blidaru [97] N. Bluhme,[38] C. Blume [63] G. Boca [21,54] F. Bock [87] T. Bodova [20] A. Bogdanov,[140] S. Boi [22] J. Bok [57] L. Boldizsár [136] A. Bolozdynya [140] M. Bombara [37] P. M. Bond [32] G. Bonomi [131,54] H. Borel [128] A. Borissov [140] A. G. Borquez Carcamo [94] H. Bossi [137] E. Botta [24] Y. E. M. Bouziani [63]

L. Bratrud [63] P. Braun-Munzinger [97] M. Bregant [110] M. Broz [35] G. E. Bruno [96,31] M. D. Buckland [23] D. Budnikov [140] H. Buesching [63] S. Bufalino [29] O. Bugnon [103] P. Buhler [102] Z. Buthelezi [67,121] S. A. Bysiak [107] M. Cai [6] H. Caines [137] A. Caliva [97] E. Calvo Villar [101] J. M. M. Camacho [109] P. Camerini [23] F. D. M. Canedo [110] M. Carabas [124] A. A. Carballo [32] F. Carnesecchi [32] R. Caron [126] L. A. D. Carvalho [110] J. Castillo Castellanos [128] F. Catalano [24,29] C. Ceballos Sanchez [141] I. Chakaberia [74] P. Chakraborty [46] S. Chandra [132] S. Chapeland [32] M. Chartier [117] S. Chattopadhyay [132] S. Chattopadhyay [99] T. G. Chavez [44] T. Cheng [97,6] C. Cheshkov [126] B. Cheynis [126] V. Chibante Barroso [32] D. D. Chinellato [111] E. S. Chizzali [95,a] J. Cho [57] S. Cho [57] P. Chochula [32] P. Christakoglou [84] C. H. Christensen [83] P. Christiansen [75] T. Chujo [123] M. Ciacco [29] C. Cicalo [51] F. Cindolo [50] M. R. Ciupek, [97] G. Clai, [50,b] F. Colamaria [49] J. S. Colburn [100] D. Colella [96,31] M. Colocci [32] M. Concas [55,c] G. Conesa Balbastre [73] Z. Conesa del Valle [72] G. Contin [23] J. G. Contreras [35] M. L. Coquet [128] T. M. Cormier, [87,d] P. Cortese [130,55] M. R. Cosentino [112] F. Costa [32] S. Costanza [21,54] C. Cot [72] J. Crkovská [94] P. Crochet [125] R. Cruz-Torres [74] E. Cuautle, [64] P. Cui [6] A. Dainese [53] M. C. Danisch [94] A. Danu [62] P. Das [80] P. Das [4] S. Das [4] A. R. Dash [135] S. Dash [46] A. De Caro [28] G. de Cataldo [49] J. de Cuveland, [38] A. De Falco [22] D. De Gruttola [28] N. De Marco [55] C. De Martin [23] S. De Pasquale [28] S. Deb [47] R. J. Debski [2] K. R. Deja [133] R. Del Grande [95] L. Dello Stritto [28] W. Deng [6] P. Dhankher [18] D. Di Bari [31] A. Di Mauro [32] R. A. Diaz [141,7] T. Dietel [113] Y. Ding [126,6] R. Divià [32] D. U. Dixit [18] Ø. Djuvsland [20] U. Dmitrieva [140] A. Dobrin [62] B. Dönigus [63] J. M. Dubinski, [133] A. Dubla [97] S. Dudi [90] P. Dupieux [125] M. Durkac [106] N. Dzalaiova, [12] T. M. Eder [135] R. J. Ehlers [87] V. N. Eikeland [20] F. Eisenhut [63] D. Elia [49] B. Erazmus [103] F. Ercolessi [25] F. Erhardt [89] M. R. Ersdal, [20] B. Espagnon [72] G. Eulisse [32] D. Evans [100] S. Evdokimov [140] L. Fabbietti [95] M. Faggin [27] J. Faivre [73] F. Fan [6] W. Fan [74] A. Fantoni [48] M. Fasel [87] P. Fecchio, [29] A. Feliciello [55] G. Feofilov [140] A. Fernández Téllez [44] L. Ferrandi [110] M. B. Ferrer [32] A. Ferrero [128] C. Ferrero [55] A. Ferretti [24] V. J. G. Feuillard [94] V. Filova [35] D. Finogeev [140] F. M. Fionda [51] F. Flor [114] A. N. Flores [108] S. Foertsch [67] I. Fokin [94] S. Fokin [140] E. Fragiacomo [56] E. Frajna [136] U. Fuchs [32] N. Funicello [28] C. Furget [73] A. Furs [140] T. Fusayasu [98] J. J. Gaardhøje [83] M. Gagliardi [24] A. M. Gago [101] C. D. Galvan [109] D. R. Gangadharan [114] P. Ganoti [78] C. Garabatos [97] J. R. A. Garcia [44] E. Garcia-Solis [9] K. Garg [103] C. Gargiulo [32] K. Garner, [135] P. Gasik [97] A. Gautam [116] M. B. Gay Ducati [65] M. Germain [103] A. Ghimouz, [123] C. Ghosh, [132] M. Giacalone [50,25] P. Giubellino [97,55] P. Giubilato [27] A. M. C. Glaenzer [128] P. Glässel [94] E. Glimos [120] D. J. Q. Goh [76] V. Gonzalez [134] L. H. González-Trueba [66] M. Gorgon [2] S. Gotovac, [33] V. Grabski [66] L. K. Graczykowski [133] E. Grecka [86] A. Grelli [58] C. Grigoras [32] V. Grigoriev [140] S. Grigoryan [141,1] F. Grosa [32] S. J. Gross-bolting, [97] J. F. Grosse-Oetringhaus [32] R. Grosso [97] D. Grund [35] G. G. Guardiano [111] R. Guernane [73] M. Guilbaud [103] K. Gulbrandsen [83] T. Gundem [63] T. Gunji [122] W. Guo [6] A. Gupta [91] R. Gupta [91] S. P. Guzman [44] L. Gyulai [136] M. K. Habib [97] C. Hadjidakis [72] F. U. Haider [91] H. Hamagaki [76] A. Hamdi [74] M. Hamid, [6] Y. Han [138] R. Hannigan [108] M. R. Haque [133] J. W. Harris [137] A. Harton [9] H. Hassan [87] D. Hatzifotiadou [50] P. Hauer [42] L. B. Havener [137] S. T. Heckel [95] E. Hellbär [97] H. Helstrup [34] M. Hemmer [63] T. Herman [35] G. Herrera Corral [8] F. Herrmann, [135] S. Herrmann [126] K. F. Hetland [34] B. Heybeck [63] H. Hillemanns [32] C. Hills [117] B. Hippolyte [127] F. W. Hoffmann, [69] B. Hofman [58] B. Hohlweger [84] G. H. Hong [138] M. Horst [95] A. Horzyk [2] R. Hosokawa, [14] Y. Hou [6] P. Hristov [32] C. Hughes [120] P. Huhn, [63] L. M. Huhta [115] C. V. Hulse [72] T. J. Humanic [88] A. Hutson [114] D. Hutter [38] J. P. Iddon [117] R. Ilkaev, [140] H. Ilyas [13] M. Inaba [123] G. M. Innocenti [32] M. Ippolitov [140] A. Isakov [86] T. Isidori [116] M. S. Islam [99] M. Ivanov, [12] M. Ivanov [97] V. Ivanov [140] M. Jablonski [2] B. Jacak [74] N. Jacazio [32] P. M. Jacobs [74] S. Jadlovska [106] J. Jadlovsky [106] S. Jaelani [82] L. Jaffe, [38] C. Jahnke [111] M. J. Jakubowska [133] M. A. Janik [133] T. Janson, [69] M. Jercic, [89] S. Jia [10] A. A. P. Jimenez [64] F. Jonas [87] J. M. Jowett [32,97] J. Jung [63] M. Jung [63] A. Junique [32] A. Jusko [100] M. J. Kabus [32,133] J. Kaewjai, [105] P. Kalinak [59] A. S. Kalteyer [97] A. Kalweit [32] V. Kaplin [140] A. Karasu Uysal [71] D. Karatovic [89] O. Karavichev [140] T. Karavicheva [140] P. Karczmarczyk [133] E. Karpechev [140] U. Kebschull [69] R. Keidel [139] D. L. D. Keijdener [58] M. Keil [32] B. Ketzer [42] A. M. Khan [6] S. Khan [15] A. Khanzadeev [140] Y. Kharlov [140] A. Khatun [116,15] A. Khuntia [107] M. B. Kidson, [113] B. Kileng [34] B. Kim [16] C. Kim [16] D. J. Kim [115] E. J. Kim [68] J. Kim [138] J. S. Kim [40] J. Kim [68] M. Kim [18,94] S. Kim [17] T. Kim [138] K. Kimura [92] S. Kirsch [63] I. Kisel [38] S. Kiselev [140] A. Kisiel [133] J. P. Kitowski [2] J. L. Klay [5] J. Klein [32] S. Klein [74] C. Klein-Bösing [135] M. Kleiner [63] T. Klemenz [95] A. Kluge [32] A. G. Knospe [114] C. Kobdaj [105] T. Kollegger, [97] A. Kondratyev [141] N. Kondratyeva [140] E. Kondratyuk [140] J. Konig [63] S. A. Konigstorfer [95] P. J. Konopka [32] G. Kornakov [133] S. D. Koryciak [2] A. Kotliarov [86] V. Kovalenko [140] M. Kowalski [107] V. Kozhuharov [36] I. Králik [59] A. Kravčáková [37] L. Kreis, [97] M. Krivda [100,59] F. Krizek [86] K. Krizkova Gajdosova [35] M. Kroesen [94] M. Krüger [63] D. M. Krupova [35] E. Kryshen [140] V. Kučera [32] C. Kuhn [127] P. G. Kuijer [84] T. Kumaoka, [123] D. Kumar, [132] L. Kumar [90] N. Kumar, [90] S. Kumar [31] S. Kundu [32] P. Kurashvili, [79] A. Kurepin [140] A. B. Kurepin [140] A. Kuryakin [140] S. Kushpil [86] J. Kvapil [100] M. J. Kweon [57] J. Y. Kwon [57] Y. Kwon [138] S. L. La Pointe [38] P. La Rocca [26] Y. S. Lai, [74] A. Lakrathok, [105] M. Lamanna [32] R. Langoy [119] P. Larionov [32] E. Laudi, [32] L. Lautner [32,95] R. Lavicka [102] T. Lazareva [140] R. Lea [131,54] H. Lee [104] G. Legras [135] J. Lehrbach [38] R. C. Lemmon [85] I. León Monzón [109] M. M. Lesch [95] E. D. Lesser [18] M. Lettrich, [95] P. Lévai [136] X. Li, [10] X. L. Li, [6] J. Lien [119] R. Lietava [100] I. Likmeta [114] B. Lim [24,16]

S. H. Lim[16] V. Lindenstruth[38] A. Lindner,[45] C. Lippmann[97] A. Liu[18] D. H. Liu[6] J. Liu[117] I. M. Lofnes[20]
C. Loizides[87] S. Lokos[107] J. Lomker[58] P. Loncar[33] J. A. Lopez[94] X. Lopez[125] E. López Torres[7] P. Lu[97,118]
J. R. Luhder[135] M. Lunardon[27] G. Luparello[56] Y. G. Ma[39] A. Maevskaya,[140] M. Mager[32] T. Mahmoud,[42]
A. Maire[127] M. V. Makariev[36] M. Malaev[140] G. Malfattore[25] N. M. Malik[91] Q. W. Malik,[19] S. K. Malik[91]
L. Malinina[141,e] D. Mal'Kevich[140] D. Mallick[80] N. Mallick[47] G. Mandaglio[30,52] V. Manko[140] F. Manso[125]
V. Manzari[49] Y. Mao[6] G. V. Margagliotti[23] A. Margotti[50] A. Marín[97] C. Markert[108] P. Martinengo[32]
J. L. Martinez,[114] M. I. Martínez[44] G. Martínez García[103] S. Masciocchi[97] M. Masera[24] A. Masoni[51]
L. Massacrier[72] A. Mastroserio[129,49] O. Matonoha[75] P. F. T. Matuoka,[110] A. Matyja[107] C. Mayer,[107]
A. L. Mazuecos[32] F. Mazzaschi[24] M. Mazzilli[32] J. E. Mdhluli[121] A. F. Mechler,[63] Y. Melikyan[43,140]
A. Menchaca-Rocha[66] E. Meninno[102,28] A. S. Menon[114] M. Meres[12] S. Mhlanga,[113,67] Y. Miake,[123]
L. Micheletti[55] L. C. Migliorin,[126] D. L. Mihaylov[95] K. Mikhaylov[141,140] A. N. Mishra[136] D. Miśkowiec[97]
A. Modak[4] A. P. Mohanty[58] B. Mohanty,[80] M. Mohisin Khan[15,f] M. A. Molander[43] Z. Moravcova[83]
C. Mordasini[95] D. A. Moreira De Godoy[135] I. Morozov[140] A. Morsch[32] T. Mrnjavac[32] V. Muccifora[48]
S. Muhuri[132] J. D. Mulligan[74] A. Mulliri,[22] M. G. Munhoz[110] R. H. Munzer[63] H. Murakami[122] S. Murray[113]
L. Musa[32] J. Musinsky[59] J. W. Myrcha[133] B. Naik[121] A. I. Nambrath[18] B. K. Nandi[46] R. Nania[50]
E. Nappi[49] A. F. Nassirpour[75] A. Nath[94] C. Nattrass[120] M. N. Naydenov[36] A. Neagu,[19] A. Negru,[124]
L. Nellen[64] S. V. Nesbo,[34] G. Neskovic[38] D. Nesterov[140] B. S. Nielsen[83] E. G. Nielsen[83] S. Nikolaev[140]
S. Nikulin[140] V. Nikulin[140] F. Noferini[50] S. Noh[11] P. Nomokonov[141] J. Norman[117] N. Novitzky[123]
P. Nowakowski[133] A. Nyanin[140] J. Nystrand[20] M. Ogino[76] A. Ohlson[75] V. A. Okorokov[140] J. Oleniacz[133]
A. C. Oliveira Da Silva[120] M. H. Oliver[137] A. Onnerstad[115] C. Oppedisano[55] A. Ortiz Velasquez[64]
J. Otwinowski[107] M. Oya[92] K. Oyama[76] Y. Pachmayer[94] S. Padhan[46] D. Pagano[131,54] G. Paić[64]
A. Palasciano[49] S. Panebianco[128] H. Park[123] H. Park[104] J. Park[57] J. E. Parkkila[32] R. N. Patra[91] B. Paul[22]
H. Pei[6] T. Peitzmann[58] X. Peng[6] M. Pennisi[24] L. G. Pereira[65] D. Peresunko[140] G. M. Perez[7] S. Perrin[128]
Y. Pestov,[140] V. Petráček[35] V. Petrov[140] M. Petrovici[45] R. P. Pezzi[103,65] S. Piano[56] M. Pikna[12] P. Pillot[103]
O. Pinazza[50,32] L. Pinsky,[114] C. Pinto[95] S. Pisano[48] M. Płoskoń[74] M. Planinic[89] F. Pliquett,[63] M. G. Poghosyan[87]
B. Polichtchouk,[140] S. Politano[29] N. Poljak[89] A. Pop[45] S. Porteboeuf-Houssais[125] V. Pozdniakov[141]
K. K. Pradhan[47] S. K. Prasad[4] S. Prasad[47] R. Preghenella[50] F. Prino[55] C. A. Pruneau[134] I. Pshenichnov[140]
M. Puccio[32] S. Pucillo[24] Z. Pugelova,[106] S. Qiu[84] L. Quaglia[24] R. E. Quishpe,[114] S. Ragoni[14,100]
A. Rakotozafindrabe[128] L. Ramello[130,55] F. Rami[127] S. A. R. Ramirez[44] T. A. Rancien,[73] M. Rasa[26]
S. S. Räsänen[43] R. Rath[50] M. P. Rauch[20] I. Ravasenga[84] K. F. Read[87,120] C. Reckziegel[112] A. R. Redelbach[38]
K. Redlich[79,g] C. A. Reetz[97] A. Rehman,[20] F. Reidt[32] H. A. Reme-Ness,[34] Z. Rescakova,[37] K. Reygers[94]
A. Riabov[140] V. Riabov[140] R. Ricci[28] M. Richter[19] A. A. Riedel[95] W. Riegler[32] C. Ristea[62]
M. Rodríguez Cahuantzi[44] K. Røed[19] R. Rogalev[140] E. Rogochaya[141] T. S. Rogoschinski[63] D. Rohr[32]
D. Röhrich[20] P. F. Rojas,[44] S. Rojas Torres[35] P. S. Rokita[133] G. Romanenko[141] F. Ronchetti[48] A. Rosano[30,52]
E. D. Rosas,[64] K. Roslon[133] A. Rossi[53] A. Roy[47] S. Roy[46] N. Rubini[25] O. V. Rueda[114,75] D. Ruggiano[133]
R. Rui[23] B. Rumyantsev,[141] P. G. Russek[2] R. Russo[84] A. Rustamov[81] E. Ryabinkin[140] Y. Ryabov[140]
A. Rybicki[107] H. Rytkonen[115] W. Rzesa[133] O. A. M. Saarimaki[43] R. Sadek[103] S. Sadhu[31] S. Sadovsky[140]
J. Saetre[20] K. Šafařík[35] S. K. Saha[4] S. Saha[80] B. Sahoo[46] R. Sahoo[47] S. Sahoo[60] D. Sahu[47] P. K. Sahu[60]
J. Saini[132] K. Sajdakova,[37] S. Sakai[123] M. P. Salvan[97] S. Sambyal[91] I. Sanna[32,95] T. B. Saramela,[110]
D. Sarkar[134] N. Sarkar,[132] P. Sarma[41] V. Sarritzu[22] V. M. Sarti[95] M. H. P. Sas[137] J. Schambach[87]
H. S. Scheid[63] C. Schiaua[45] R. Schicker[94] A. Schmah,[94] C. Schmidt[97] H. R. Schmidt,[93] M. O. Schmidt[32]
M. Schmidt,[93] N. V. Schmidt[87] A. R. Schmier[120] R. Schotter[127] A. Schröter[38] J. Schukraft[32] K. Schwarz,[97]
K. Schweda[97] G. Scioli[25] E. Scomparin[55] J. E. Seger[14] Y. Sekiguchi,[122] D. Sekihata[122] I. Selyuzhenkov[97,140]
S. Senyukov[127] J. J. Seo[57] D. Serebryakov[140] L. Šerkšnytė[95] A. Sevcenco[62] T. J. Shaba[67] A. Shabetai[103]
R. Shahoyan,[32] A. Shangaraev[140] A. Sharma,[90] B. Sharma[91] D. Sharma[46] H. Sharma[107] M. Sharma[91]
S. Sharma[76] S. Sharma[91] U. Sharma[91] A. Shatat[72] O. Sheibani,[114] K. Shigaki[92] M. Shimomura,[77] J. Shin,[11]
S. Shirinkin[140] Q. Shou[39] Y. Sibiriak[140] S. Siddhanta[51] T. Siemiarczuk[79] T. F. Silva[110] D. Silvermyr[75]
T. Simantathammakul,[105] R. Simeonov[36] B. Singh,[91] B. Singh[95] R. Singh[80] R. Singh[91] R. Singh[47] S. Singh[15]
V. K. Singh[132] V. Singhal[132] T. Sinha[99] B. Sitar[12] M. Sitta[130,55] T. B. Skaali,[19] G. Skorodumovs[94]
M. Slupecki[43] N. Smirnov[137] R. J. M. Snellings[58] E. H. Solheim[19] J. Song[114] A. Songmoolnak,[105] F. Soramel[27]
R. Spijkers[84] I. Sputowska[107] J. Staa[75] J. Stachel[94] I. Stan[62] P. J. Steffanic[120] S. F. Stiefelmaier[94]
D. Stocco[103] I. Storehaug[19] P. Stratmann[135] S. Strazzi[25] C. P. Stylianidis,[84] A. A. P. Suaide[110] C. Suire[72]
M. Sukhanov[140] M. Suljic[32] R. Sultanov[140] V. Sumberia[91] S. Sumowidagdo[82] S. Swain[60] I. Szarka[12]
M. Szymkowski[133] S. F. Taghavi[95] G. Taillepied[97] J. Takahashi[111] G. J. Tambave[20] S. Tang[125,6] Z. Tang[118]
J. D. Tapia Takaki[116] N. Tapus,[124] L. A. Tarasovicova[135] M. G. Tarzila[45] G. F. Tassielli[31] A. Tauro[32]
G. Tejeda Muñoz[44] A. Telesca[32] L. Terlizzi[24] C. Terrevoli[114] G. Tersimonov,[3] S. Thakur[4] D. Thomas[108]
A. Tikhonov[140] A. R. Timmins[114] M. Tkacik,[106] T. Tkacik[106] A. Toia[63] R. Tokumoto,[92] N. Topilskaya[140]
M. Toppi[48] F. Torales-Acosta,[18] T. Tork[72] A. G. Torres Ramos[31] A. Trifiró[30,52] A. S. Triolo[30,52] S. Tripathy[50]

T. Tripathy [46] S. Trogolo [32] V. Trubnikov [3] W. H. Trzaska [115] T. P. Trzcinski [133] A. Tumkin [140] R. Turrisi [53] T. S. Tveter [19] K. Ullaland [20] B. Ulukutlu [95] A. Uras [126] M. Urioni [54,131] G. L. Usai [22] M. Vala [37] N. Valle [21] L. V. R. van Doremalen [58] M. van Leeuwen [84] C. A. van Veen [94] R. J. G. van Weelden [84] P. Vande Vyvre [32] D. Varga [136] Z. Varga [136] M. Vasileiou [78] A. Vasiliev [140] O. Vázquez Doce [48] V. Vechernin [140] E. Vercellin [24] S. Vergara Limón [44] L. Vermunt [97] R. Vértesi [136] M. Verweij [58] L. Vickovic [33] Z. Vilakazi [121] O. Villalobos Baillie [100] A. Villani [23] G. Vino [49] A. Vinogradov [140] T. Virgili [28] V. Vislavicius [75] A. Vodopyanov [141] B. Volkel [32] M. A. Völkl [94] K. Voloshin [140] S. A. Voloshin [134] G. Volpe [31] B. von Haller [32] I. Vorobyev [95] N. Vozniuk [140] J. Vrláková [37] C. Wang [39] D. Wang [39] Y. Wang [39] A. Wegrzynek [32] F. T. Weiglhofer [38] S. C. Wenzel [32] J. P. Wessels [135] S. L. Weyhmiller [137] J. Wiechula [63] J. Wikne [19] G. Wilk [79] J. Wilkinson [97] G. A. Willems [135] B. Windelband [94] M. Winn [128] J. R. Wright [108] W. Wu [39] Y. Wu [118] R. Xu [6] A. Yadav [42] A. K. Yadav [132] S. Yalcin [71] Y. Yamaguchi [92] S. Yang [20] S. Yano [92] Z. Yin [6] I.-K. Yoo [16] J. H. Yoon [57] S. Yuan [20] A. Yuncu [94] V. Zaccolo [23] C. Zampolli [32] F. Zanone [94] N. Zardoshti [32,100] A. Zarochentsev [140] P. Závada [61] N. Zaviyalov [140] M. Zhalov [140] B. Zhang [6] L. Zhang [39] S. Zhang [39] X. Zhang [6] Y. Zhang [118] Z. Zhang [6] M. Zhao [10] V. Zherebchevskii [140] Y. Zhi [10] D. Zhou [6] Y. Zhou [83] J. Zhu [97,6] Y. Zhu [6] S. C. Zugravel [55] and N. Zurlo [131,54]

(ALICE Collaboration)

[1]*A.I. Alikhanyan National Science Laboratory (Yerevan Physics Institute) Foundation, Yerevan, Armenia*
[2]*AGH University of Science and Technology, Cracow, Poland*
[3]*Bogolyubov Institute for Theoretical Physics, National Academy of Sciences of Ukraine, Kiev, Ukraine*
[4]*Bose Institute, Department of Physics and Centre for Astroparticle Physics and Space Science (CAPSS), Kolkata, India*
[5]*California Polytechnic State University, San Luis Obispo, California, United States*
[6]*Central China Normal University, Wuhan, China*
[7]*Centro de Aplicaciones Tecnológicas y Desarrollo Nuclear (CEADEN), Havana, Cuba*
[8]*Centro de Investigación y de Estudios Avanzados (CINVESTAV), Mexico City and Mérida, Mexico*
[9]*Chicago State University, Chicago, Illinois, United States*
[10]*China Institute of Atomic Energy, Beijing, China*
[11]*Chungbuk National University, Cheongju, Republic of Korea*
[12]*Comenius University Bratislava, Faculty of Mathematics, Physics and Informatics, Bratislava, Slovak Republic*
[13]*COMSATS University Islamabad, Islamabad, Pakistan*
[14]*Creighton University, Omaha, Nebraska, United States*
[15]*Department of Physics, Aligarh Muslim University, Aligarh, India*
[16]*Department of Physics, Pusan National University, Pusan, Republic of Korea*
[17]*Department of Physics, Sejong University, Seoul, Republic of Korea*
[18]*Department of Physics, University of California, Berkeley, California, United States*
[19]*Department of Physics, University of Oslo, Oslo, Norway*
[20]*Department of Physics and Technology, University of Bergen, Bergen, Norway*
[21]*Dipartimento di Fisica, Università di Pavia, Pavia, Italy*
[22]*Dipartimento di Fisica dell'Università and Sezione INFN, Cagliari, Italy*
[23]*Dipartimento di Fisica dell'Università and Sezione INFN, Trieste, Italy*
[24]*Dipartimento di Fisica dell'Università and Sezione INFN, Turin, Italy*
[25]*Dipartimento di Fisica e Astronomia dell'Università and Sezione INFN, Bologna, Italy*
[26]*Dipartimento di Fisica e Astronomia dell'Università and Sezione INFN, Catania, Italy*
[27]*Dipartimento di Fisica e Astronomia dell'Università and Sezione INFN, Padova, Italy*
[28]*Dipartimento di Fisica 'E.R. Caianiello' dell'Università and Gruppo Collegato INFN, Salerno, Italy*
[29]*Dipartimento DISAT del Politecnico and Sezione INFN, Turin, Italy*
[30]*Dipartimento di Scienze MIFT, Università di Messina, Messina, Italy*
[31]*Dipartimento Interateneo di Fisica 'M. Merlin' and Sezione INFN, Bari, Italy*
[32]*European Organization for Nuclear Research (CERN), Geneva, Switzerland*
[33]*Faculty of Electrical Engineering, Mechanical Engineering and Naval Architecture, University of Split, Split, Croatia*
[34]*Faculty of Engineering and Science, Western Norway University of Applied Sciences, Bergen, Norway*
[35]*Faculty of Nuclear Sciences and Physical Engineering, Czech Technical University in Prague, Prague, Czech Republic*
[36]*Faculty of Physics, Sofia University, Sofia, Bulgaria*
[37]*Faculty of Science, P.J. Šafárik University, Košice, Slovak Republic*
[38]*Frankfurt Institute for Advanced Studies, Johann Wolfgang Goethe-Universität Frankfurt, Frankfurt, Germany*
[39]*Fudan University, Shanghai, China*
[40]*Gangneung-Wonju National University, Gangneung, Republic of Korea*
[41]*Gauhati University, Department of Physics, Guwahati, India*

[42] *Helmholtz-Institut für Strahlen- und Kernphysik, Rheinische Friedrich-Wilhelms-Universität Bonn, Bonn, Germany*

[43] *Helsinki Institute of Physics (HIP), Helsinki, Finland*

[44] *High Energy Physics Group, Universidad Autónoma de Puebla, Puebla, Mexico*

[45] *Horia Hulubei National Institute of Physics and Nuclear Engineering, Bucharest, Romania*

[46] *Indian Institute of Technology Bombay (IIT), Mumbai, India*

[47] *Indian Institute of Technology Indore, Indore, India*

[48] *INFN, Laboratori Nazionali di Frascati, Frascati, Italy*

[49] *INFN, Sezione di Bari, Bari, Italy*

[50] *INFN, Sezione di Bologna, Bologna, Italy*

[51] *INFN, Sezione di Cagliari, Cagliari, Italy*

[52] *INFN, Sezione di Catania, Catania, Italy*

[53] *INFN, Sezione di Padova, Padova, Italy*

[54] *INFN, Sezione di Pavia, Pavia, Italy*

[55] *INFN, Sezione di Torino, Turin, Italy*

[56] *INFN, Sezione di Trieste, Trieste, Italy*

[57] *Inha University, Incheon, Republic of Korea*

[58] *Institute for Gravitational and Subatomic Physics (GRASP), Utrecht University/Nikhef, Utrecht, Netherlands*

[59] *Institute of Experimental Physics, Slovak Academy of Sciences, Košice, Slovak Republic*

[60] *Institute of Physics, Homi Bhabha National Institute, Bhubaneswar, India*

[61] *Institute of Physics of the Czech Academy of Sciences, Prague, Czech Republic*

[62] *Institute of Space Science (ISS), Bucharest, Romania*

[63] *Institut für Kernphysik, Johann Wolfgang Goethe-Universität Frankfurt, Frankfurt, Germany*

[64] *Instituto de Ciencias Nucleares, Universidad Nacional Autónoma de México, Mexico City, Mexico*

[65] *Instituto de Física, Universidade Federal do Rio Grande do Sul (UFRGS), Porto Alegre, Brazil*

[66] *Instituto de Física, Universidad Nacional Autónoma de México, Mexico City, Mexico*

[67] *iThemba LABS, National Research Foundation, Somerset West, South Africa*

[68] *Jeonbuk National University, Jeonju, Republic of Korea*

[69] *Johann-Wolfgang-Goethe Universität Frankfurt Institut für Informatik, Fachbereich Informatik und Mathematik, Frankfurt, Germany*

[70] *Korea Institute of Science and Technology Information, Daejeon, Republic of Korea*

[71] *KTO Karatay University, Konya, Turkey*

[72] *Laboratoire de Physique des 2 Infinis, Irène Joliot-Curie, Orsay, France*

[73] *Laboratoire de Physique Subatomique et de Cosmologie, Université Grenoble-Alpes, CNRS-IN2P3, Grenoble, France*

[74] *Lawrence Berkeley National Laboratory, Berkeley, California, United States*

[75] *Lund University Department of Physics, Division of Particle Physics, Lund, Sweden*

[76] *Nagasaki Institute of Applied Science, Nagasaki, Japan*

[77] *Nara Women's University (NWU), Nara, Japan*

[78] *National and Kapodistrian University of Athens, School of Science, Department of Physics, Athens, Greece*

[79] *National Centre for Nuclear Research, Warsaw, Poland*

[80] *National Institute of Science Education and Research, Homi Bhabha National Institute, Jatni, India*

[81] *National Nuclear Research Center, Baku, Azerbaijan*

[82] *National Research and Innovation Agency - BRIN, Jakarta, Indonesia*

[83] *Niels Bohr Institute, University of Copenhagen, Copenhagen, Denmark*

[84] *Nikhef, National institute for subatomic physics, Amsterdam, Netherlands*

[85] *Nuclear Physics Group, STFC Daresbury Laboratory, Daresbury, United Kingdom*

[86] *Nuclear Physics Institute of the Czech Academy of Sciences, Husinec-Řež, Czech Republic*

[87] *Oak Ridge National Laboratory, Oak Ridge, Tennessee, United States*

[88] *Ohio State University, Columbus, Ohio, United States*

[89] *Physics department, Faculty of science, University of Zagreb, Zagreb, Croatia*

[90] *Physics Department, Panjab University, Chandigarh, India*

[91] *Physics Department, University of Jammu, Jammu, India*

[92] *Physics Program and International Institute for Sustainability with Knotted Chiral Meta Matter (SKCM2), Hiroshima University, Hiroshima, Japan*

[93] *Physikalisches Institut, Eberhard-Karls-Universität Tübingen, Tübingen, Germany*

[94] *Physikalisches Institut, Ruprecht-Karls-Universität Heidelberg, Heidelberg, Germany*

[95] *Physik Department, Technische Universität München, Munich, Germany*

[96] *Politecnico di Bari and Sezione INFN, Bari, Italy*

[97] *Research Division and ExtreMe Matter Institute EMMI, GSI Helmholtzzentrum für Schwerionenforschung GmbH, Darmstadt, Germany*

[98] *Saga University, Saga, Japan*

[99] *Saha Institute of Nuclear Physics, Homi Bhabha National Institute, Kolkata, India*

^{100}*School of Physics and Astronomy, University of Birmingham, Birmingham, United Kingdom*

^{101}*Sección Física, Departamento de Ciencias, Pontificia Universidad Católica del Perú, Lima, Peru*

^{102}*Stefan Meyer Institut für Subatomare Physik (SMI), Vienna, Austria*

^{103}*SUBATECH, IMT Atlantique, Nantes Université, CNRS-IN2P3, Nantes, France*

^{104}*Sungkyunkwan University, Suwon City, Republic of Korea*

^{105}*Suranaree University of Technology, Nakhon Ratchasima, Thailand*

^{106}*Technical University of Košice, Košice, Slovak Republic*

^{107}*The Henryk Niewodniczanski Institute of Nuclear Physics, Polish Academy of Sciences, Cracow, Poland*

^{108}*The University of Texas at Austin, Austin, Texas, United States*

^{109}*Universidad Autónoma de Sinaloa, Culiacán, Mexico*

^{110}*Universidade de São Paulo (USP), São Paulo, Brazil*

^{111}*Universidade Estadual de Campinas (UNICAMP), Campinas, Brazil*

^{112}*Universidade Federal do ABC, Santo Andre, Brazil*

^{113}*University of Cape Town, Cape Town, South Africa*

^{114}*University of Houston, Houston, Texas, United States*

^{115}*University of Jyväskylä, Jyväskylä, Finland*

^{116}*University of Kansas, Lawrence, Kansas, United States*

^{117}*University of Liverpool, Liverpool, United Kingdom*

^{118}*University of Science and Technology of China, Hefei, China*

^{119}*University of South-Eastern Norway, Kongsberg, Norway*

^{120}*University of Tennessee, Knoxville, Tennessee, United States*

^{121}*University of the Witwatersrand, Johannesburg, South Africa*

^{122}*University of Tokyo, Tokyo, Japan*

^{123}*University of Tsukuba, Tsukuba, Japan*

^{124}*University Politehnica of Bucharest, Bucharest, Romania*

^{125}*Université Clermont Auvergne, CNRS/IN2P3, LPC, Clermont-Ferrand, France*

^{126}*Université de Lyon, CNRS/IN2P3, Institut de Physique des 2 Infinis de Lyon, Lyon, France*

^{127}*Université de Strasbourg, CNRS, IPHC UMR 7178, F-67000 Strasbourg, France, Strasbourg, France*

^{128}*Université Paris-Saclay Centre d'Etudes de Saclay (CEA), IRFU, Départment de Physique Nucléaire (DPhN), Saclay, France*

^{129}*Università degli Studi di Foggia, Foggia, Italy*

^{130}*Università del Piemonte Orientale, Vercelli, Italy*

^{131}*Università di Brescia, Brescia, Italy*

^{132}*Variable Energy Cyclotron Centre, Homi Bhabha National Institute, Kolkata, India*

^{133}*Warsaw University of Technology, Warsaw, Poland*

^{134}*Wayne State University, Detroit, Michigan, United States*

^{135}*Westfälische Wilhelms-Universität Münster, Institut für Kernphysik, Münster, Germany*

^{136}*Wigner Research Centre for Physics, Budapest, Hungary*

^{137}*Yale University, New Haven, Connecticut, United States*

^{138}*Yonsei University, Seoul, Republic of Korea*

^{139}*Zentrum für Technologie und Transfer (ZTT), Worms, Germany*

^{140}*Affiliated with an institute covered by a cooperation agreement with CERN*

^{141}*Affiliated with an international laboratory covered by a cooperation agreement with CERN*

[a]Also at: Max-Planck-Institut für Physik, Munich, Germany.

[b]Also at: Italian National Agency for New Technologies, Energy and Sustainable Economic Development (ENEA), Bologna, Italy.

[c]Also at: Dipartimento DET del Politecnico di Torino, Turin, Italy.

[d]Deceased.

[e]Also at: An institution covered by a cooperation agreement with CERN.

[f]Also at: Department of Applied Physics, Aligarh Muslim University, Aligarh, India.

[g]Also at: Institute of Theoretical Physics, University of Wroclaw, Poland.